



Angular analysis of the $B^+ \rightarrow K^{*+} \mu^+ \mu^-$ decay

LHCb collaboration[†]

Abstract

We present an angular analysis of the $B^+ \rightarrow K^{*+}(\rightarrow K_S^0 \pi^+) \mu^+ \mu^-$ decay using 9 fb^{-1} of pp collision data collected with the LHCb experiment. For the first time, the full set of CP -averaged angular observables is measured in intervals of the dimuon invariant mass squared. Local deviations from Standard Model predictions are observed, similar to those in previous LHCb analyses of the isospin-partner $B^0 \rightarrow K^{*0} \mu^+ \mu^-$ decay. The global tension is dependent on which effective couplings are considered and on the choice of theory nuisance parameters.

Published in Phys. Rev. Lett. **126**, 161802 (2021)

© 2021 CERN for the benefit of the LHCb collaboration. CC BY 4.0 licence.

[†]Authors are listed at the end of this Letter.

Transitions between b quarks and s quarks with the emission of two charged leptons, $\ell^+\ell^-$, only proceed through loop-level processes. Such decays are therefore sensitive to possible contributions from heavy mediators that are inaccessible to direct-production searches. Recent studies of $b \rightarrow s\ell^+\ell^-$ branching fractions [1–5], angular distributions [1, 4, 6–13] and ratios of branching fractions between decays with different flavours of lepton pairs [14–18] show discrepancies with respect to the predictions of the Standard Model (SM). While these deviations can be consistently explained by the presence of contributions from additional vector or axial-vector currents [19–37], effects from uncertainties related to hadronic form factors or long-distance contributions cannot be ruled out [38–42].

The $B \rightarrow K^*\mu^+\mu^-$ decay, where K^* denotes the $K^*(892)$ meson, has been the subject of extensive studies [7, 12, 43, 44]. A large number of these decays are recorded at the LHC experiments and the flavour of the B meson can be identified from the $K^* \rightarrow K\pi$ decay products. This allows the full set of angular observables of the $B \rightarrow K^*\mu^+\mu^-$ decay to be studied. A recent study [12] of the $B^0 \rightarrow K^{*0}\mu^+\mu^-$ decay channel by the LHCb collaboration confirmed the tension in the angular observables with respect to the SM predictions.

This letter reports the first measurement of the complete set of angular observables in the isospin partner decay $B^+ \rightarrow K^{*+}\mu^+\mu^-$, with the K^{*+} meson reconstructed through the decay chain $K^{*+} \rightarrow K_S^0\pi^+$ with $K_S^0 \rightarrow \pi^+\pi^-$. Charge-conjugation is implied throughout this letter. This decay is mediated by the same underlying processes as the $B^0 \rightarrow K^{*0}\mu^+\mu^-$ decay, while potentially receiving additional contributions from $\bar{b} \rightarrow \bar{u}W^+$ transitions, leading to the emission of a K^{*+} meson [45]. Furthermore, any deviation from isospin symmetry, as reported previously in the $B \rightarrow K^*\gamma$ decay [46], could result in a difference in the angular distributions between the isospin partners. In the SM, however, isospin-breaking effects are expected to be small. The analysis uses the data set collected by the LHCb collaboration in the years 2011, 2012 (Run 1) and 2015–2018 (Run 2), at centre-of-mass energies of 7, 8 and 13 TeV, respectively. The data set corresponds to an integrated luminosity of 9 fb^{-1} .

The LHCb detector [47, 48] is a single-arm forward spectrometer covering the pseudorapidity range $2 < \eta < 5$, designed for the study of particles containing b or c quarks. The detector includes a high-precision tracking system consisting of a silicon-strip vertex detector surrounding the pp interaction region [49], a large-area silicon-strip detector located upstream of a dipole magnet with a bending power of about 4 Tm, and three stations of silicon-strip detectors and straw drift tubes [50, 51] placed downstream of the magnet. The tracking system provides a measurement of the momentum, p , of charged particles with a relative uncertainty that varies from 0.5% at low momentum to 1.0% at 200 GeV/ c . The minimum distance of a track to a primary pp collision vertex (PV), the impact parameter, is measured with a resolution of $(15 + 29/p_T) \mu\text{m}$, where p_T is the component of the momentum transverse to the beam, in GeV/ c . Different types of charged hadrons are distinguished using information from two ring-imaging Cherenkov detectors [52]. Photons, electrons and hadrons are identified by a calorimeter system consisting of scintillating-pad and preshower detectors, an electromagnetic and a hadronic calorimeter. Muons are identified by a system composed of alternating layers of iron and multiwire proportional chambers [53]. The online event selection is performed by a trigger [54, 55], which consists of a hardware stage, based on information from the calorimeter and muon systems, followed by a software stage, which applies a full event reconstruction.

Simulated decays are used to model the effects of the reconstruction and the candidate selection. In the simulation, pp collisions are generated using PYTHIA [56] with a specific LHCb configuration [57]. Decays of unstable particles are described by EVTGEN [58], in which final-state radiation is generated using PHOTOS [59]. The interaction of the generated particles with the detector, and its response, are implemented using the GEANT4 toolkit [60], as described in Ref. [61]. Corrections to the simulation are applied to account for mismodelling in the p_T spectrum of the B^+ mesons and the multiplicity of tracks in the event. The corrections are obtained from a background-subtracted data sample of $B^+ \rightarrow (J/\psi \rightarrow \mu^+\mu^-) K^{*+}$ decays.

In the first two stages of the trigger, the event is selected based on kinematical and geometrical properties of the muons. In the last trigger stage, dimuon or topological trigger algorithms are used to select the B^+ candidate. The $K_S^0 \rightarrow \pi^+\pi^-$ decays are reconstructed in two different categories: the *long* category involves short-lived K_S^0 candidates for which the pions are reconstructed in the vertex detector; the *downstream* category comprises K_S^0 candidates that decay later such that track segments of the pions can only be reconstructed in tracking detectors downstream of the vertex locator. The K_S^0 candidates reconstructed in the long category have better mass, momentum and vertex resolution than those in the downstream category, where the latter has a larger sample size than the former. The K_S^0 candidates are required to have an invariant mass within $30 \text{ MeV}/c^2$ of the known K_S^0 mass [62].

The $K^{*+} \rightarrow K_S^0\pi^+$ decay is reconstructed by combining a K_S^0 candidate with a charged pion and requiring their invariant mass to be within $100 \text{ MeV}/c^2$ of the world average of the K^{*+} mass [62]. The $B^+ \rightarrow K^{*+}\mu^+\mu^-$ candidates are formed by combining the K^{*+} candidate with two well-identified, oppositely charged muons. The B^+ candidates are required to have an invariant mass, $m(K_S^0\pi^+\mu^+\mu^-)$, in the range $5150\text{--}6000 \text{ MeV}/c^2$. The lower value of the mass window is chosen to reject background from partially reconstructed $B \rightarrow K_S^0\pi^+\pi^+\mu^-\mu^-$ decays. Dimuon pairs having invariant mass squared, q^2 , around the $\phi(1020)$ ($0.98 < q^2 < 1.1 \text{ GeV}^2/c^4$), J/ψ ($8.0 < q^2 < 11.0 \text{ GeV}^2/c^4$) and $\psi(2S)$ ($12.5 < q^2 < 15.0 \text{ GeV}^2/c^4$) resonances are vetoed. All tracks in the final state are required to have a significant impact parameter with respect to any PV and the B^+ candidate decay vertex needs to be well displaced from any PV in the event. A kinematical fit [63] is performed to the full decay chain, in which the reconstructed K_S^0 mass is constrained to the known value [62].

Decays of B^0 mesons to the $K_S^0\mu^+\mu^-$ final state with a pion added can form a peaking structure in the B^+ mass window. Therefore, candidates with an invariant mass $m(K_S^0\mu^+\mu^-)$ within $50 \text{ MeV}/c^2$ of the known B^0 mass are vetoed. Background originating from $B^+ \rightarrow (J/\psi \rightarrow \mu^+\mu^-) K^{*+}$ decays is probed by testing the $K_S^0\pi^+$ and dimuon invariant masses formed by exchanging the particle hypotheses between the pion from the K^{*+} meson decay and the muon with the same charge. The candidates with a dimuon mass within $50 \text{ MeV}/c^2$ of the J/ψ meson mass and a $K_S^0\pi^+$ invariant mass within $30 \text{ MeV}/c^2$ of the K^{*+} mass are then rejected. The background from B decays with two hadrons misidentified as muons is negligible.

To increase the signal-to-background ratio, a multivariate classification is employed. The data are split into four subsets, according to the Run 1 and Run 2 data-taking periods and the category of the K_S^0 meson. A boosted decision tree with gradient boosting [64, 65] from the TMVA toolkit [66] is then trained on each data set individually, using simulated events as a proxy for signal and candidates with $m(K_S^0\pi^+\mu^+\mu^-)$ larger than $5400 \text{ MeV}/c^2$

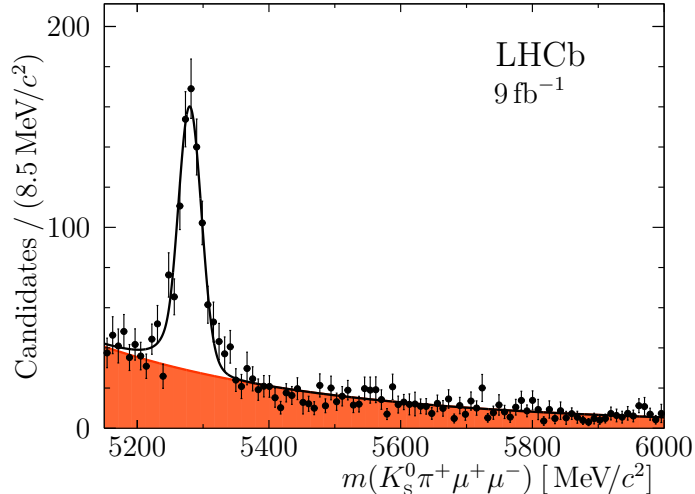


Figure 1: Distribution of the $K_S^0 \pi^+ \mu^+ \mu^-$ invariant mass. The black points represent the full data set, while the solid curve shows the fit result. The background component is represented by the orange shaded area.

as a proxy for background. The variables include kinematical and topological properties of the final state or intermediate particles, the quality of the vertex of the B^+ candidate, and an isolation criterion related to the asymmetry in p_T between all tracks inside a cone around the flight directions of the B^+ candidates and the tracks associated to the B^+ decay products [67]. Figure 1 shows the B^+ -candidate invariant mass distribution, $m(K_S^0 \pi^+ \mu^+ \mu^-)$, for all the selected data. A fit model with a double-sided Crystal Ball function for the signal and an exponential function for the background component is overlaid. The number of $B^+ \rightarrow K^{*+} \mu^+ \mu^-$ signal candidates from this fit is 737 ± 34 , where the uncertainty is statistical only.

Ignoring the natural width of the K^{*+} meson, the decay $B^+ \rightarrow K^{*+} \mu^+ \mu^-$ can be fully described by four variables: q^2 and the set of three angles $\vec{\Omega} = (\theta_\ell, \theta_K, \phi)$. The angle between the μ^+ (μ^-) and the direction opposite to that of the B^+ (B^-) in the rest frame of the dimuon system is denoted θ_ℓ . The angle between the direction of the K_S^0 and the B^+ (B^-) in the rest frame of the K^{*+} (K^{*-}) system is denoted θ_K . The angle ϕ is the angle between the plane defined by the momenta of the muon pair and the plane defined by the kaon and pion momenta in the B^+ (B^-) rest frame. A full description of the angular basis is given in Ref. [44].

Averaging over B^+ and B^- decays, with rates respectively denoted Γ and $\bar{\Gamma}$, the differential decay rate of the $B^+ \rightarrow K^{*+} \mu^+ \mu^-$ decay with the $K_S^0 \pi^+$ system in a P-wave configuration is

$$\begin{aligned}
\frac{1}{d(\Gamma + \bar{\Gamma})/dq^2} \frac{d^4(\Gamma + \bar{\Gamma})}{dq^2 d\vec{\Omega}} \Big|_{\text{P}} &= \frac{9}{32\pi} \left[\frac{3}{4}(1 - F_L) \sin^2 \theta_K + F_L \cos^2 \theta_K \right. \\
&\quad + \frac{1}{4}(1 - F_L) \sin^2 \theta_K \cos 2\theta_\ell \\
&\quad - F_L \cos^2 \theta_K \cos 2\theta_\ell + S_3 \sin^2 \theta_K \sin^2 \theta_\ell \cos 2\phi \\
&\quad + S_4 \sin 2\theta_K \sin 2\theta_\ell \cos \phi + S_5 \sin 2\theta_K \sin \theta_\ell \cos \phi \\
&\quad + \frac{4}{3} A_{\text{FB}} \sin^2 \theta_K \cos \theta_\ell + S_7 \sin 2\theta_K \sin \theta_\ell \sin \phi \\
&\quad \left. + S_8 \sin 2\theta_K \sin 2\theta_\ell \sin \phi + S_9 \sin^2 \theta_K \sin^2 \theta_\ell \sin 2\phi \right], \tag{1}
\end{aligned}$$

where F_L is the fraction of the longitudinally polarised K^{*+} mesons, A_{FB} is the forward-backward asymmetry of the dimuon system and S_i are other CP -averaged observables [7].

The $K_S^0 \pi^+$ system can also be in an S-wave configuration, which modifies the differential decay rate to

$$\begin{aligned}
\frac{1}{d(\Gamma + \bar{\Gamma})/dq^2} \frac{d^4(\Gamma + \bar{\Gamma})}{dq^2 d\vec{\Omega}} \Big|_{\text{P+S}} &= (1 - F_S) \frac{1}{d(\Gamma + \bar{\Gamma})/dq^2} \frac{d^4(\Gamma + \bar{\Gamma})}{dq^2 d\vec{\Omega}} \Big|_{\text{P}} \\
&\quad + \frac{3}{16\pi} F_S \sin^2 \theta_l \\
&\quad + \frac{9}{32\pi} (S_{11} + S_{13} \cos 2\theta_l) \cos \theta_K \\
&\quad + \frac{9}{32\pi} (S_{14} \sin 2\theta_l + S_{15} \sin \theta_l) \sin \theta_K \cos \phi \\
&\quad + \frac{9}{32\pi} (S_{16} \sin \theta_l + S_{17} \sin 2\theta_l) \sin \theta_K \sin \phi, \tag{2}
\end{aligned}$$

where F_S denotes the S-wave fraction and the coefficients S_{11} , S_{13} – S_{17} arise from interference between the S- and P-wave amplitudes. Throughout this letter, F_S and the interference coefficients are treated as nuisance parameters. In addition to the observable basis comprising F_L , A_{FB} and S_3 – S_9 , a basis with so-called optimised observables, denoted $P_i^{(\prime)}$, for which the leading form-factor uncertainties cancel [68], is used. The notation for the $P_i^{(\prime)}$ observables is defined in Ref. [43].

Due to the limited number of signal candidates, the observables cannot all be measured simultaneously. A folding procedure is therefore employed that uses symmetries of the differential decay rate in the angles to cancel some observables, reducing the number of free parameters in the fit. By performing different folds, all angular observables can be studied, without any loss in precision. Five different folds are used to study the observables A_{FB} and S_9 (P_2 and P_3), S_4 (P'_4), S_5 (P'_5), S_7 (P'_6) and S_8 (P'_8), respectively. The observables F_L and S_3 (P_1) are measured in each fold. This procedure is detailed in Ref. [69] and was previously used in Refs. [8–10, 43, 44]. The values of F_L and S_3 (P_1) are taken from the same fold that is used to extract the value of S_8 (P'_8), as the number of free parameters in the fit is the smallest in this fold.

The angular observables are extracted using an unbinned maximum-likelihood fit to the B^+ candidate mass and the three decay angles in intervals of q^2 . The eight narrow and two

wide q^2 intervals are identical to those in Refs. [7,12]. The angular distributions are fitted with the function described in Eq. (2) for the signal, and with second-order polynomials in $\cos\theta_K$ and $\cos\theta_\ell$ for the background. The background in the ϕ angle is uniform. No significant correlation is observed between the angular background distributions in the B^+ candidate mass sidebands, justifying a factorisation of the background description in the three decay angles.

The reconstruction and selection efficiency varies over the angular and q^2 phase space. This acceptance effect is parametrised before folding using the sum over the product of four one-dimensional Legendre polynomials, each depending on one angle or q^2 . This is analogous to the procedure used in Ref. [12]. The effect is corrected using weights derived from simulation. The weight then corresponds to the inverse of the efficiency. No dependence of the acceptance effect on the K^{*+} candidate mass is observed.

Given the low signal yield and narrow q^2 intervals, the S-wave fraction F_S cannot be determined with sufficient precision to guarantee unbiased results for the P-wave angular observables. Therefore, a two-dimensional unbinned maximum-likelihood fit to $m(K_S^0\pi^+\mu^+\mu^-)$ and the K^{*+} candidate mass $m(K_S^0\pi^+)$ is first performed in three q^2 intervals: 1.1–8.0, 11.0–12.5 and 15.0–19.0 GeV²/c⁴. The $m(K_S^0\pi^+\mu^+\mu^-)$ distribution is fitted using the signal and background model described above. The K^{*+} candidate mass is fitted using a relativistic Breit-Wigner function to describe the P-wave component, the LASS parametrisation to describe the S-wave component [70] and a linear function to describe the combinatorial background. S- and P-wave interference terms are neglected in this treatment. The value of F_S in the default narrow q^2 intervals is then computed by multiplying the value of F_S in the broad intervals with the ratio between F_L in the narrow and broad intervals. This procedure assumes a similar q^2 dependence of the longitudinal component of the P wave and the S wave and is broadly compatible with the results from Ref. [5]. Given the weak dependence of the P-wave observables on the value of F_S , this procedure ensures unbiased results without relying on values of F_S from an external measurement. Pseudoexperiments indicate that determining F_S in this manner induces at most a bias of 13% of the statistical uncertainty on the angular observables. This is treated as a systematic uncertainty. All values of F_S are measured to be positive and compatible with the results in Ref. [5].

Fitting the folded data set only provides statistical correlations between observables measured in the same fold. In order to obtain the correlations between all observables, the bootstrapping technique [71] is used to produce a large number of pseudodata sets. The measurement of the observables in each fold of these pseudodata sets enables computing the correlations between observables in different folds. The statistical precision of the elements of the correlation matrix is determined to be around 0.11. In order to ensure correct coverage in the presence of physical boundaries of the observables, the statistical uncertainty for each observable in each q^2 interval for the signal channel is evaluated using the Feldman-Cousins technique [72].

The full analysis procedure with acceptance correction, extraction of F_S and extraction of the angular observables, is tested on a sample of $B^+ \rightarrow J/\psi K^{*+}$ decays with the same selection as applied to the signal channel, but requiring the dimuon invariant mass squared to be in the range 8.68–10.09 GeV²/c⁴. The results are found to be in good agreement with previous measurements from the BaBar [73], Belle [74] and LHCb [75] experiments.

Several sources of systematic uncertainties are considered and their sizes are estimated using pseudoexperiments. Various contributions to the overall systematic uncertainty

are related to the correction of acceptance effects. They include the limited size of the simulation sample and the parametrisation of the acceptance function. Other systematic uncertainties are related to the correction of differences between data and simulation, the model of the B^+ candidate mass distribution and angular background, the impact of the $B^0 \rightarrow K_S^0 \mu^+ \mu^-$ veto on the mass distribution of the combinatorial background, the angular resolution and the effect of constraining the value of F_S with a two-dimensional fit. Pseudoexperiments are used to assess a possible bias introduced by the fit procedure. The pseudodata samples are generated based on the result of the fit to data or on the predictions from either the SM or a new physics scenario favoured by the LHCb measurement from Ref. [12] with the real part of the Wilson coefficient C_9 shifted by -1 with respect to SM predictions. Here, C_9 is the strength of the vector coupling in an effective field theory of b quark to s quark transitions. The largest bias observed is 33% of the statistical uncertainty for S_4 in the q^2 interval 4.0–6.0 GeV $^2/c^4$. Given that the biases can depend on the values of the observables themselves, the largest biases observed among the three pseudodata samples are taken as systematic uncertainties. The potential exchange of the π^+ mesons from the decays of the K^{*+} and K_S^0 candidates and the angular background description differing between the upper and lower mass sidebands are both considered as further sources of systematic uncertainty. Both effects are found to be negligible. All systematic uncertainties are added in quadrature and their total size is reported together with the numerical results of the observables in Sec. 2 of the Supplemental Material. A summary of the contributions from the various sources is given in Table 23 of the Supplemental Material. The statistical uncertainty dominates for all q^2 intervals and all observables, which implies that correlations with the results from Ref. [12] are negligible.

The results of the angular fits for the observables $P_2 = \frac{2}{3} A_{\text{FB}} / (1 - F_L)$ and $P_5' = S_5 / \sqrt{F_L(1 - F_L)}$ are shown in Fig. 2. They are compared with the two SM predictions taken from Ref. [76] with hadronic form factors from Refs. [77–79], and from Refs. [80, 81] with hadronic form factors from Ref. [82]. The rest of the observables are presented in Figs. 3 and 4 in the Supplemental Material to this letter. The numerical results of the angular fits to the data are presented in Tables 1 and 2, where values for the two wide q^2 intervals are also given. The correlations are given in Tables 3–12 and 13–22 for the S_i and $P_i^{(\prime)}$ observables, respectively.

The majority of observables show good agreement with the SM predictions, F_L and A_{FB} agree well with the measurements in Ref. [13]. The largest local discrepancy is in the measurement of P_2 in the 6.0–8.0 GeV $^2/c^4$ interval, where a deviation of 3.0σ with respect to the SM prediction is observed. The pattern of deviations from the SM predictions in the observables S_5 (P_5') and A_{FB} (P_2) broadly agrees with the deviations observed in the $B^0 \rightarrow K^{*0} \mu^+ \mu^-$ channel.

The FLAVIO package [83] (version 2.0.0) is used to perform a fit to the angular observables varying the parameter $\text{Re}(C_9)$, which is motivated by Refs. [7, 12]. In order to minimise the theoretical uncertainties related to contributions from virtual charm-quark loops [82] and broad charmonium resonances [84–86], the narrow q^2 intervals up to 6.0 GeV $^2/c^4$ plus the wide q^2 interval $15.0 < q^2 < 19.0$ GeV $^2/c^4$ are included in the fit. The default FLAVIO SM nuisance parameters are used, including form-factor parameters and subleading corrections to account for long-distance QCD interference effects with the charmonium decay modes [76, 77]. The best-fit point results in a shift with respect to the SM value of $\text{Re}(C_9)$ of -1.9 and gives a tension with the SM of 3.1σ . However, the tension observed depends on the q^2 intervals considered, which effective couplings are

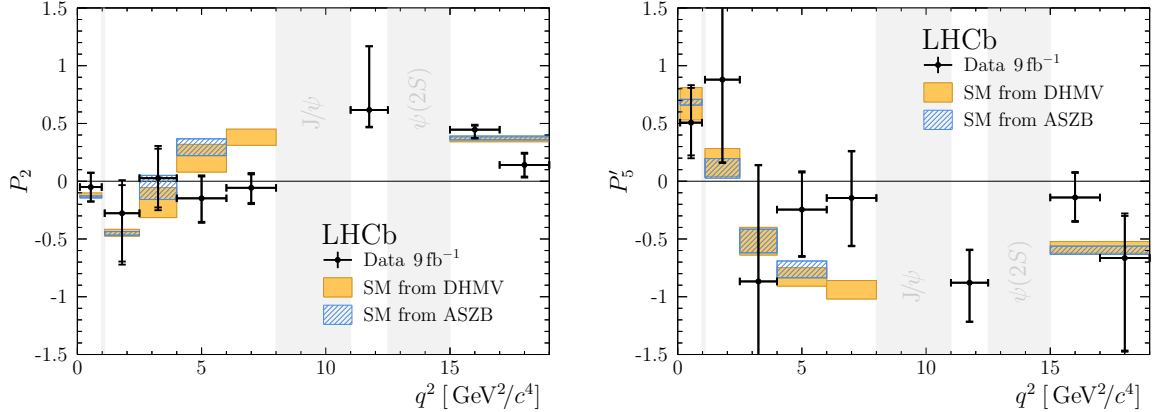


Figure 2: The CP -averaged observables (left) P_2 and (right) P_5' in intervals of q^2 . The first (second) error bars represent the statistical (total) uncertainties. The theoretical predictions in blue are based on Ref. [76] with hadronic form factors taken from Refs. [77–79] and are obtained with the FLAVIO software package [83] (version 2.0.0). The theoretical predictions in orange are based on Refs. [80,81] with hadronic form factors from Ref. [82]. The grey bands indicate the regions of excluded $\phi(1020)$, J/ψ and $\psi(2S)$ resonances.

varied and the handling of the SM nuisance parameters.

In summary, using the complete pp data set collected with the LHCb experiment in Runs 1 and 2, the full set of angular observables for the decay $B^+ \rightarrow K^{*+} \mu^+ \mu^-$ is measured for the first time. The results confirm the global tension with respect to the SM predictions previously reported in the decay $B^0 \rightarrow K^{*0} \mu^+ \mu^-$.

Acknowledgements

We express our gratitude to our colleagues in the CERN accelerator departments for the excellent performance of the LHC. We thank the technical and administrative staff at the LHCb institutes. We acknowledge support from CERN and from the national agencies: CAPES, CNPq, FAPERJ and FINEP (Brazil); MOST and NSFC (China); CNRS/IN2P3 (France); BMBF, DFG and MPG (Germany); INFN (Italy); NWO (Netherlands); MNiSW and NCN (Poland); MEN/IFA (Romania); MSHE (Russia); MICINN (Spain); SNSF and SER (Switzerland); NASU (Ukraine); STFC (United Kingdom); DOE NP and NSF (USA). We acknowledge the computing resources that are provided by CERN, IN2P3 (France), KIT and DESY (Germany), INFN (Italy), SURF (Netherlands), PIC (Spain), GridPP (United Kingdom), RRCKI and Yandex LLC (Russia), CSCS (Switzerland), IFIN-HH (Romania), CBPF (Brazil), PL-GRID (Poland) and OSC (USA). We are indebted to the communities behind the multiple open-source software packages on which we depend. Individual groups or members have received support from AvH Foundation (Germany); EPLANET, Marie Skłodowska-Curie Actions and ERC (European Union); A*MIDEX, ANR, Labex P2IO and OCEVU, and Région Auvergne-Rhône-Alpes (France); Key Research Program of Frontier Sciences of CAS, CAS PIFI, CAS CCEPP, Fundamental Research Funds for the Central Universities, and Sci. & Tech. Program of Guangzhou (China); RFBR, RSF and Yandex LLC (Russia); GVA, XuntaGal and GENCAT (Spain); the Royal Society and the Leverhulme Trust (United Kingdom).

Supplemental Material

This supplemental material includes additional information to that already provided in the main letter.

The full set of results for both sets of angular observables is presented in graphical form in Sec. 1 and in tabular form in Sec. 2. The correlations between the angular observables are given in Sec. 3 and Sec. 4 for S_i and $P_i^{(\prime)}$ observables, respectively. A summary of the systematic uncertainties is given in Sec. 5. The signal yields in each q^2 interval are given in Table 24. The projections of the data in $m(K_S^0\pi^+\mu^+\mu^-)$, $\cos\theta_K$, $\cos\theta_\ell$ and ϕ using the angular fold with the transformation $\phi \rightarrow \phi + \pi$, for $\phi < 0$, are given in Figs. 5 - 8 along with the fitted probability density functions.

1 Graphical results for the S_i and $P_i^{(\prime)}$ observables

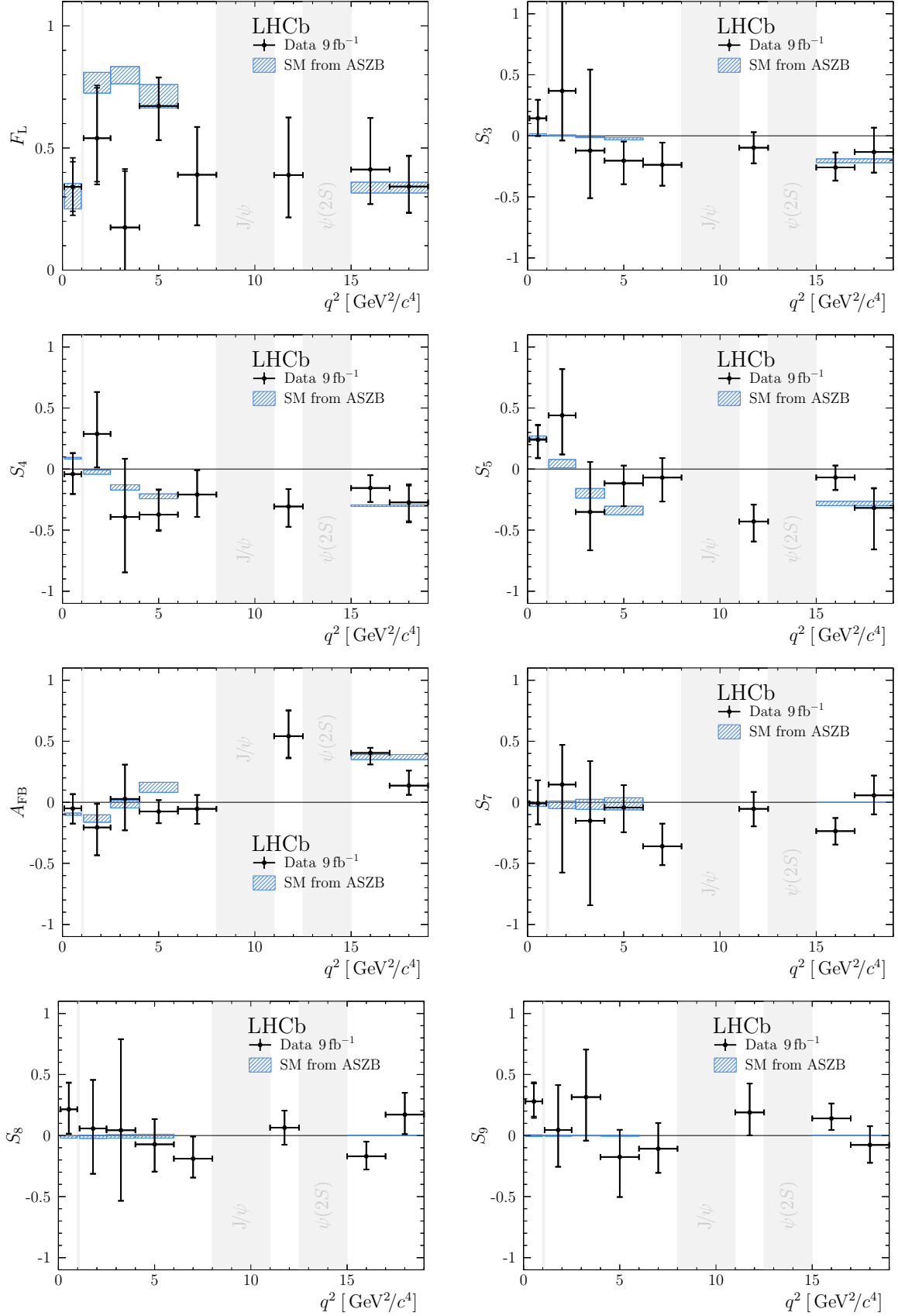


Figure 3: The CP -averaged observables F_L , A_{FB} and S_3 – S_9 versus q^2 . The first (second) error bars represent the statistical (total) uncertainties. The theoretical predictions are based on Refs. [76–79]. The grey bands indicate regions of excluded resonances.

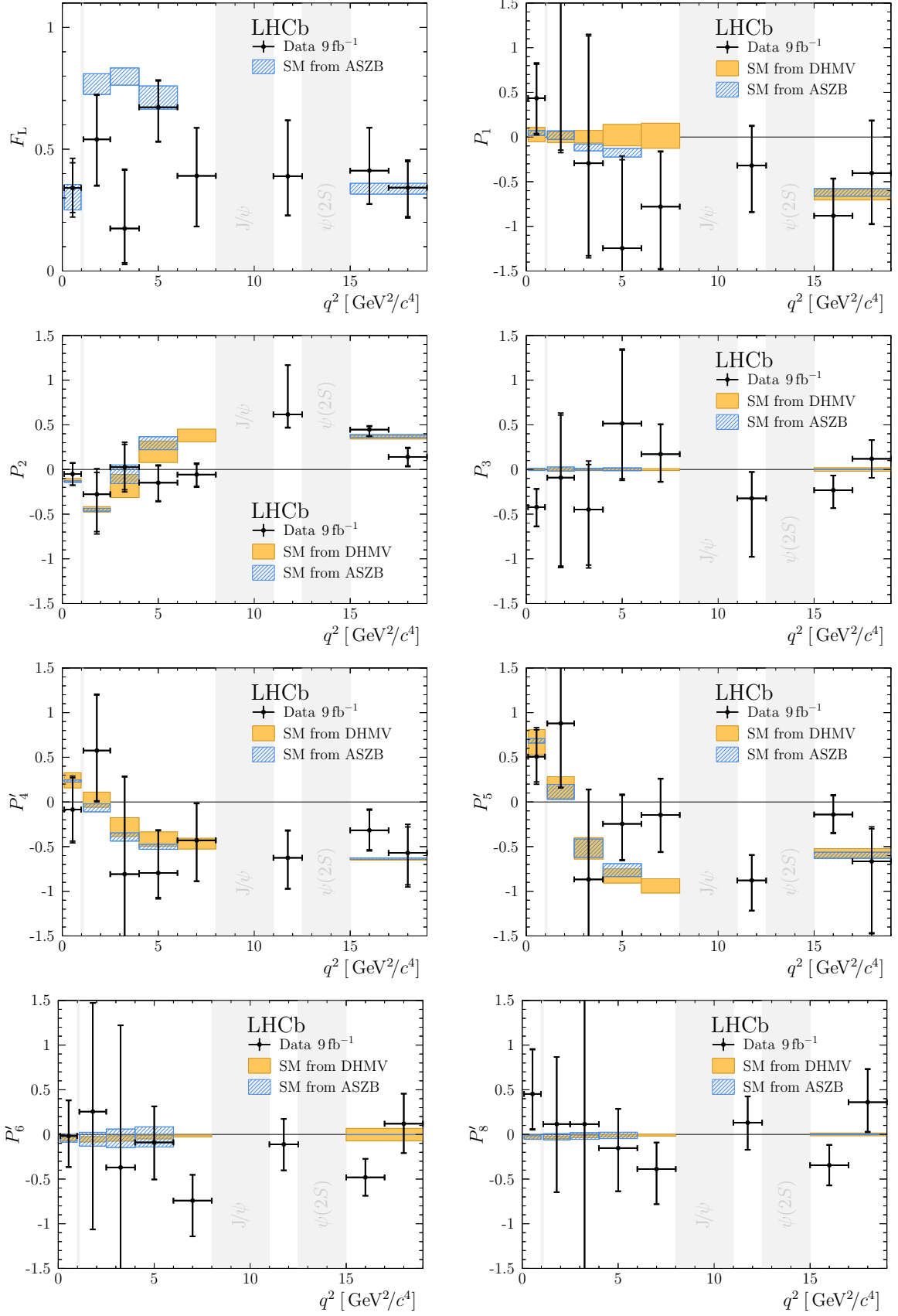


Figure 4: The optimised observables P_1 to P_8 versus q^2 . The first (second) error bars represent the statistical (total) uncertainties. The theoretical predictions are based on Refs. [80–82] (orange) and on Refs. [76–79] (blue). The grey bands indicate regions of excluded resonances.

2 Tabular results for the S_i and $P_i^{(\prime)}$ observables

Table 1: Results for the CP -averaged observables F_L , A_{FB} and S_3 – S_9 . The first uncertainties are statistical and the second systematic.

q^2 [GeV $^2/c^4$]	F_L	S_3	S_4	S_5
[0.10, 0.98]	$0.34^{+0.10}_{-0.10} \pm 0.06$	$0.14^{+0.15}_{-0.14} \pm 0.02$	$-0.04^{+0.17}_{-0.16} \pm 0.04$	$0.24^{+0.12}_{-0.15} \pm 0.04$
[1.1, 2.5]	$0.54^{+0.21}_{-0.18} \pm 0.06$	$0.37^{+0.97}_{-0.41} \pm 0.03$	$0.29^{+0.34}_{-0.27} \pm 0.03$	$0.44^{+0.38}_{-0.32} \pm 0.05$
[2.5, 4.0]	$0.17^{+0.23}_{-0.32} \pm 0.06$	$-0.12^{+0.66}_{-0.39} \pm 0.02$	$-0.39^{+0.48}_{-0.45} \pm 0.04$	$-0.35^{+0.41}_{-0.31} \pm 0.02$
[4.0, 6.0]	$0.67^{+0.12}_{-0.14} \pm 0.02$	$-0.20^{+0.16}_{-0.19} \pm 0.01$	$-0.37^{+0.20}_{-0.13} \pm 0.05$	$-0.12^{+0.14}_{-0.19} \pm 0.03$
[6.0, 8.0]	$0.39^{+0.20}_{-0.21} \pm 0.01$	$-0.24^{+0.18}_{-0.17} \pm 0.02$	$-0.21^{+0.20}_{-0.18} \pm 0.02$	$-0.07^{+0.16}_{-0.20} \pm 0.02$
[11.0, 12.5]	$0.39^{+0.24}_{-0.17} \pm 0.02$	$-0.10^{+0.13}_{-0.13} \pm 0.02$	$-0.31^{+0.14}_{-0.17} \pm 0.02$	$-0.43^{+0.14}_{-0.16} \pm 0.02$
[15.0, 17.0]	$0.41^{+0.21}_{-0.14} \pm 0.02$	$-0.26^{+0.12}_{-0.11} \pm 0.03$	$-0.16^{+0.10}_{-0.11} \pm 0.02$	$-0.07^{+0.10}_{-0.10} \pm 0.03$
[17.0, 19.0]	$0.34^{+0.12}_{-0.11} \pm 0.03$	$-0.13^{+0.20}_{-0.17} \pm 0.04$	$-0.27^{+0.14}_{-0.15} \pm 0.06$	$-0.32^{+0.16}_{-0.34} \pm 0.04$
[1.1, 6.0]	$0.59^{+0.09}_{-0.09} \pm 0.03$	$-0.10^{+0.11}_{-0.11} \pm 0.01$	$-0.20^{+0.13}_{-0.14} \pm 0.03$	$-0.04^{+0.12}_{-0.12} \pm 0.02$
[15.0, 19.0]	$0.40^{+0.13}_{-0.11} \pm 0.03$	$-0.21^{+0.09}_{-0.09} \pm 0.03$	$-0.19^{+0.10}_{-0.13} \pm 0.06$	$-0.12^{+0.07}_{-0.07} \pm 0.02$

q^2 [GeV $^2/c^4$]	A_{FB}	S_7	S_8	S_9
[0.10, 0.98]	$-0.05^{+0.12}_{-0.12} \pm 0.03$	$-0.01^{+0.19}_{-0.17} \pm 0.01$	$0.21^{+0.22}_{-0.20} \pm 0.05$	$0.28^{+0.15}_{-0.12} \pm 0.06$
[1.1, 2.5]	$-0.21^{+0.19}_{-0.23} \pm 0.04$	$0.15^{+0.32}_{-0.72} \pm 0.02$	$0.06^{+0.40}_{-0.37} \pm 0.04$	$0.05^{+0.37}_{-0.30} \pm 0.02$
[2.5, 4.0]	$0.03^{+0.28}_{-0.26} \pm 0.01$	$-0.15^{+0.49}_{-0.69} \pm 0.03$	$0.04^{+0.75}_{-0.58} \pm 0.03$	$0.31^{+0.39}_{-0.36} \pm 0.02$
[4.0, 6.0]	$-0.08^{+0.09}_{-0.10} \pm 0.01$	$-0.04^{+0.18}_{-0.20} \pm 0.01$	$-0.07^{+0.21}_{-0.22} \pm 0.03$	$-0.18^{+0.22}_{-0.33} \pm 0.02$
[6.0, 8.0]	$-0.05^{+0.11}_{-0.12} \pm 0.01$	$-0.36^{+0.18}_{-0.15} \pm 0.02$	$-0.19^{+0.18}_{-0.16} \pm 0.02$	$-0.11^{+0.21}_{-0.20} \pm 0.02$
[11.0, 12.5]	$0.54^{+0.21}_{-0.18} \pm 0.05$	$-0.05^{+0.14}_{-0.14} \pm 0.01$	$0.06^{+0.14}_{-0.14} \pm 0.01$	$0.19^{+0.24}_{-0.19} \pm 0.03$
[15.0, 17.0]	$0.40^{+0.04}_{-0.09} \pm 0.01$	$-0.24^{+0.11}_{-0.11} \pm 0.02$	$-0.17^{+0.12}_{-0.11} \pm 0.02$	$0.14^{+0.12}_{-0.09} \pm 0.02$
[17.0, 19.0]	$0.14^{+0.12}_{-0.07} \pm 0.02$	$0.06^{+0.16}_{-0.16} \pm 0.01$	$0.17^{+0.18}_{-0.16} \pm 0.02$	$-0.08^{+0.15}_{-0.15} \pm 0.02$
[1.1, 6.0]	$-0.08^{+0.07}_{-0.08} \pm 0.02$	$-0.10^{+0.11}_{-0.13} \pm 0.01$	$0.02^{+0.13}_{-0.14} \pm 0.02$	$-0.05^{+0.11}_{-0.12} \pm 0.01$
[15.0, 19.0]	$0.31^{+0.06}_{-0.06} \pm 0.04$	$-0.14^{+0.08}_{-0.09} \pm 0.01$	$-0.06^{+0.09}_{-0.09} \pm 0.01$	$0.04^{+0.08}_{-0.06} \pm 0.02$

Table 2: Results for the optimised observables F_L and $P_1-P'_8$. The first uncertainties are statistical and the second systematic.

q^2 [GeV ² /c ⁴]	F_L	P_1	P_2	P_3
[0.10, 0.98]	$0.34^{+0.10}_{-0.10} \pm 0.06$	$0.44^{+0.38}_{-0.40} \pm 0.11$	$-0.05^{+0.12}_{-0.12} \pm 0.03$	$-0.42^{+0.20}_{-0.21} \pm 0.05$
[1.1, 2.5]	$0.54^{+0.18}_{-0.19} \pm 0.03$	$1.60^{+4.92}_{-1.75} \pm 0.32$	$-0.28^{+0.24}_{-0.42} \pm 0.15$	$-0.09^{+0.70}_{-0.99} \pm 0.18$
[2.5, 4.0]	$0.17^{+0.24}_{-0.14} \pm 0.04$	$-0.29^{+1.43}_{-1.04} \pm 0.22$	$0.03^{+0.26}_{-0.25} \pm 0.11$	$-0.45^{+0.50}_{-0.62} \pm 0.20$
[4.0, 6.0]	$0.67^{+0.11}_{-0.14} \pm 0.03$	$-1.24^{+0.99}_{-1.17} \pm 0.29$	$-0.15^{+0.19}_{-0.20} \pm 0.06$	$0.52^{+0.82}_{-0.62} \pm 0.15$
[6.0, 8.0]	$0.39^{+0.20}_{-0.21} \pm 0.02$	$-0.78^{+0.61}_{-0.69} \pm 0.10$	$-0.06^{+0.12}_{-0.13} \pm 0.05$	$0.17^{+0.33}_{-0.31} \pm 0.06$
[11.0, 12.5]	$0.39^{+0.23}_{-0.16} \pm 0.03$	$-0.32^{+0.44}_{-0.52} \pm 0.09$	$0.62^{+0.55}_{-0.14} \pm 0.04$	$-0.32^{+0.29}_{-0.65} \pm 0.05$
[15.0, 17.0]	$0.41^{+0.18}_{-0.14} \pm 0.02$	$-0.88^{+0.41}_{-0.67} \pm 0.07$	$0.45^{+0.03}_{-0.07} \pm 0.03$	$-0.23^{+0.16}_{-0.20} \pm 0.02$
[17.0, 19.0]	$0.34^{+0.11}_{-0.12} \pm 0.04$	$-0.40^{+0.58}_{-0.57} \pm 0.09$	$0.14^{+0.10}_{-0.10} \pm 0.04$	$0.12^{+0.21}_{-0.21} \pm 0.02$
[1.1, 6.0]	$0.59^{+0.10}_{-0.10} \pm 0.03$	$-0.51^{+0.56}_{-0.54} \pm 0.08$	$-0.13^{+0.13}_{-0.13} \pm 0.05$	$0.12^{+0.27}_{-0.28} \pm 0.04$
[15.0, 19.0]	$0.40^{+0.13}_{-0.11} \pm 0.02$	$-0.70^{+0.35}_{-0.43} \pm 0.07$	$0.34^{+0.09}_{-0.07} \pm 0.04$	$-0.07^{+0.12}_{-0.13} \pm 0.03$

q^2 [GeV ² /c ⁴]	P'_4	P'_5	P'_6	P'_8
[0.10, 0.98]	$-0.09^{+0.36}_{-0.35} \pm 0.12$	$0.51^{+0.30}_{-0.28} \pm 0.12$	$-0.02^{+0.40}_{-0.34} \pm 0.06$	$0.45^{+0.50}_{-0.39} \pm 0.09$
[1.1, 2.5]	$0.58^{+0.62}_{-0.56} \pm 0.11$	$0.88^{+0.70}_{-0.71} \pm 0.10$	$0.25^{+1.22}_{-1.32} \pm 0.08$	$0.12^{+0.75}_{-0.76} \pm 0.05$
[2.5, 4.0]	$-0.81^{+1.09}_{-0.84} \pm 0.14$	$-0.87^{+1.00}_{-1.68} \pm 0.09$	$-0.37^{+1.59}_{-3.91} \pm 0.05$	$0.12^{+7.89}_{-4.95} \pm 0.07$
[4.0, 6.0]	$-0.79^{+0.47}_{-0.28} \pm 0.09$	$-0.25^{+0.32}_{-0.40} \pm 0.09$	$-0.09^{+0.40}_{-0.41} \pm 0.05$	$-0.15^{+0.44}_{-0.48} \pm 0.05$
[6.0, 8.0]	$-0.43^{+0.41}_{-0.45} \pm 0.06$	$-0.15^{+0.40}_{-0.41} \pm 0.06$	$-0.74^{+0.29}_{-0.40} \pm 0.03$	$-0.39^{+0.30}_{-0.39} \pm 0.02$
[11.0, 12.5]	$-0.63^{+0.30}_{-0.34} \pm 0.07$	$-0.88^{+0.28}_{-0.34} \pm 0.05$	$-0.11^{+0.28}_{-0.29} \pm 0.03$	$0.13^{+0.29}_{-0.30} \pm 0.04$
[15.0, 17.0]	$-0.32^{+0.23}_{-0.22} \pm 0.08$	$-0.14^{+0.21}_{-0.20} \pm 0.06$	$-0.48^{+0.21}_{-0.21} \pm 0.02$	$-0.34^{+0.23}_{-0.22} \pm 0.04$
[17.0, 19.0]	$-0.57^{+0.29}_{-0.36} \pm 0.13$	$-0.66^{+0.36}_{-0.80} \pm 0.13$	$0.12^{+0.33}_{-0.33} \pm 0.04$	$0.36^{+0.37}_{-0.33} \pm 0.07$
[1.1, 6.0]	$-0.41^{+0.28}_{-0.28} \pm 0.07$	$-0.07^{+0.25}_{-0.25} \pm 0.04$	$-0.21^{+0.23}_{-0.23} \pm 0.04$	$0.03^{+0.26}_{-0.28} \pm 0.06$
[15.0, 19.0]	$-0.39^{+0.18}_{-0.21} \pm 0.10$	$-0.24^{+0.16}_{-0.16} \pm 0.05$	$-0.28^{+0.19}_{-0.14} \pm 0.03$	$-0.11^{+0.19}_{-0.18} \pm 0.03$

3 Correlation matrices for the S_i observables

Correlation matrices between the CP -averaged observables F_L , A_{FB} and S_3 – S_9 in the different q^2 intervals are provided in Tables 3–12. Correlations between observables measured with different folds are obtained using the bootstrapping technique [71]. The different q^2 intervals are statistically independent.

Table 3: Correlation matrix for the CP -averaged observables F_L , A_{FB} and S_3 – S_9 from the maximum-likelihood fit in the interval $0.10 < q^2 < 0.98 \text{ GeV}^2/c^4$.

	F_L	S_3	S_4	S_5	A_{FB}	S_7	S_8	S_9
F_L	1	0.04	−0.01	0.03	0.04	0.12	−0.00	−0.11
S_3		1	−0.02	0.12	−0.02	0.02	0.06	0.02
S_4			1	−0.27	−0.09	−0.25	0.24	−0.06
S_5				1	0.10	0.22	−0.18	0.06
A_{FB}					1	0.19	−0.27	−0.06
S_7						1	−0.35	0.22
S_8							1	−0.08
S_9								1

Table 4: Correlation matrix for the CP -averaged observables F_L , A_{FB} and S_3 – S_9 from the maximum-likelihood fit in the interval $1.1 < q^2 < 2.5 \text{ GeV}^2/c^4$.

	F_L	S_3	S_4	S_5	A_{FB}	S_7	S_8	S_9
F_L	1	0.16	−0.05	0.11	0.11	0.04	−0.10	−0.03
S_3		1	0.06	0.09	−0.02	0.13	−0.01	−0.12
S_4			1	−0.02	0.17	0.05	0.33	0.09
S_5				1	0.20	0.22	−0.06	0.04
A_{FB}					1	0.20	0.11	0.12
S_7						1	0.06	0.16
S_8							1	0.22
S_9								1

Table 5: Correlation matrix for the CP -averaged observables F_L , A_{FB} and S_3 – S_9 from the maximum-likelihood fit in the interval $2.5 < q^2 < 4.0 \text{ GeV}^2/c^4$.

	F_L	S_3	S_4	S_5	A_{FB}	S_7	S_8	S_9
F_L	1	0.02	−0.01	0.06	−0.08	−0.02	−0.07	0.04
S_3		1	0.02	−0.06	−0.01	−0.03	0.07	0.02
S_4			1	0.00	−0.06	0.10	−0.05	−0.00
S_5				1	0.01	−0.07	0.00	−0.11
A_{FB}					1	0.05	0.06	−0.16
S_7						1	0.26	−0.14
S_8							1	−0.09
S_9								1

Table 6: Correlation matrix for the CP -averaged observables F_L , A_{FB} and S_3 – S_9 from the maximum-likelihood fit in the interval $4.0 < q^2 < 6.0 \text{ GeV}^2/c^4$.

	F_L	S_3	S_4	S_5	A_{FB}	S_7	S_8	S_9
F_L	1	0.20	-0.09	-0.09	0.07	0.01	0.16	-0.03
S_3		1	-0.08	-0.10	0.03	0.11	0.17	0.03
S_4			1	-0.08	-0.15	0.07	-0.04	0.05
S_5				1	-0.17	-0.02	0.09	-0.02
A_{FB}					1	-0.04	-0.03	-0.01
S_7						1	0.09	0.09
S_8							1	-0.08
S_9								1

Table 7: Correlation matrix for the CP -averaged observables F_L , A_{FB} and S_3 – S_9 from the maximum-likelihood fit in the interval $6.0 < q^2 < 8.0 \text{ GeV}^2/c^4$.

	F_L	S_3	S_4	S_5	A_{FB}	S_7	S_8	S_9
F_L	1	0.26	-0.01	0.07	0.01	-0.04	0.06	0.05
S_3		1	0.01	-0.03	-0.05	0.08	-0.04	-0.00
S_4			1	0.35	0.02	-0.05	-0.03	-0.10
S_5				1	0.02	-0.11	-0.07	-0.17
A_{FB}					1	-0.05	-0.19	-0.13
S_7						1	-0.10	-0.06
S_8							1	0.04
S_9								1

Table 8: Correlation matrix for the CP -averaged observables F_L , A_{FB} and S_3 – S_9 from the maximum-likelihood fit in the interval $11.0 < q^2 < 12.5 \text{ GeV}^2/c^4$.

	F_L	S_3	S_4	S_5	A_{FB}	S_7	S_8	S_9
F_L	1	0.09	0.03	0.09	-0.44	-0.09	-0.13	-0.08
S_3		1	-0.08	-0.13	-0.08	-0.04	-0.04	-0.19
S_4			1	0.08	0.06	-0.05	-0.09	0.12
S_5				1	-0.30	0.05	-0.04	-0.10
A_{FB}					1	0.10	0.11	0.15
S_7						1	0.05	-0.07
S_8							1	-0.07
S_9								1

Table 9: Correlation matrix for the CP -averaged observables F_L , A_{FB} and S_3 – S_9 from the maximum-likelihood fit in the interval $15.0 < q^2 < 17.0 \text{ GeV}^2/c^4$.

	F_L	S_3	S_4	S_5	A_{FB}	S_7	S_8	S_9
F_L	1	0.19	0.04	0.07	-0.28	-0.06	-0.13	-0.07
S_3		1	-0.09	-0.06	0.04	0.01	-0.06	0.01
S_4			1	0.27	0.07	0.10	0.06	0.14
S_5				1	-0.15	0.09	-0.06	-0.13
A_{FB}					1	0.07	-0.02	0.16
S_7						1	0.23	0.02
S_8							1	0.00
S_9								1

Table 10: Correlation matrix for the CP -averaged observables F_L , A_{FB} and S_3 – S_9 from the maximum-likelihood fit in the interval $17.0 < q^2 < 19.0 \text{ GeV}^2/c^4$.

	F_L	S_3	S_4	S_5	A_{FB}	S_7	S_8	S_9
F_L	1	-0.10	-0.02	-0.10	-0.10	0.07	-0.10	-0.01
S_3		1	-0.08	0.06	0.09	0.01	0.08	-0.02
S_4			1	-0.06	-0.07	0.00	0.06	0.04
S_5				1	-0.19	-0.03	0.09	0.02
A_{FB}					1	0.17	0.01	-0.07
S_7						1	-0.17	0.10
S_8							1	-0.19
S_9								1

Table 11: Correlation matrix for the CP -averaged observables F_L , A_{FB} and S_3 – S_9 from the maximum-likelihood fit in the interval $1.1 < q^2 < 6.0 \text{ GeV}^2/c^4$.

	F_L	S_3	S_4	S_5	A_{FB}	S_7	S_8	S_9
F_L	1	0.17	-0.00	-0.02	0.01	0.04	0.08	0.06
S_3		1	-0.01	-0.02	-0.02	0.04	-0.03	-0.05
S_4			1	-0.03	0.06	-0.02	0.19	-0.01
S_5				1	0.01	0.14	0.04	0.04
A_{FB}					1	-0.05	0.04	0.05
S_7						1	0.17	-0.02
S_8							1	-0.01
S_9								1

Table 12: Correlation matrix for the CP -averaged observables F_L , A_{FB} and S_3 – S_9 from the maximum-likelihood fit in the interval $15.0 < q^2 < 19.0 \text{ GeV}^2/c^4$.

	F_L	S_3	S_4	S_5	A_{FB}	S_7	S_8	S_9
F_L	1	0.13	-0.05	-0.02	-0.17	-0.02	0.03	-0.05
S_3		1	-0.07	-0.00	-0.02	0.12	0.10	-0.05
S_4			1	0.05	-0.14	0.06	0.05	-0.02
S_5				1	0.05	-0.07	0.07	-0.05
A_{FB}					1	-0.10	-0.03	0.10
S_7						1	0.15	-0.01
S_8							1	-0.09
S_9								1

4 Correlation matrices for the $P_i^{(\prime)}$ observables

Correlation matrices between the CP -averaged observables P_i in the different q^2 intervals are provided in Tables 13–22. Correlations between observables measured with different folds are obtained using the bootstrapping technique [71]. The different q^2 intervals are statistically independent.

Table 13: Correlation matrix for the CP -averaged observables F_L and $P_i^{(\prime)}$ from the maximum-likelihood fit in the interval $0.10 < q^2 < 0.98 \text{ GeV}^2/c^4$.

	F_L	P_1	P_2	P_3	P'_4	P'_5	P'_6	P'_8
F_L	1	-0.14	0.02	-0.18	-0.03	0.00	0.12	-0.01
P_1		1	-0.00	-0.01	-0.03	0.17	0.01	0.03
P_2			1	0.02	-0.08	0.09	0.19	-0.24
P_3				1	0.06	-0.03	-0.21	0.04
P'_4					1	-0.22	-0.23	0.15
P'_5						1	0.18	-0.18
P'_6							1	-0.25
P'_8								1

Table 14: Correlation matrix for the CP -averaged observables F_L and $P_i^{(\prime)}$ from the maximum-likelihood fit in the interval $1.1 < q^2 < 2.5 \text{ GeV}^2/c^4$.

	F_L	P_1	P_2	P_3	P'_4	P'_5	P'_6	P'_8
F_L	1	0.03	0.02	-0.01	-0.06	-0.01	0.05	-0.08
P_1		1	-0.05	-0.01	0.06	-0.09	-0.03	0.04
P_2			1	-0.05	0.15	0.12	0.10	0.13
P_3				1	-0.08	-0.07	-0.02	-0.13
P'_4					1	0.03	-0.01	0.22
P'_5						1	0.09	-0.08
P'_6							1	-0.01
P'_8								1

Table 15: Correlation matrix for the CP -averaged observables F_L and $P_i^{(\prime)}$ from the maximum-likelihood fit in the interval $2.5 < q^2 < 4.0 \text{ GeV}^2/c^4$.

	F_L	P_1	P_2	P_3	P'_4	P'_5	P'_6	P'_8
F_L	1	0.00	0.00	0.02	-0.02	-0.03	-0.06	-0.03
P_1		1	0.00	0.04	0.04	0.00	-0.04	-0.06
P_2			1	0.07	-0.01	0.04	0.04	-0.03
P_3				1	-0.03	0.02	0.06	-0.01
P'_4					1	0.07	0.06	0.08
P'_5						1	-0.02	-0.09
P'_6							1	0.21
P'_8								1

Table 16: Correlation matrix for the CP -averaged observables F_L and $P_i^{(\prime)}$ from the maximum-likelihood fit in the interval $4.0 < q^2 < 6.0 \text{ GeV}^2/c^4$.

	F_L	P_1	P_2	P_3	P'_4	P'_5	P'_6	P'_8
F_L	1	0.16	-0.10	0.02	-0.02	-0.08	0.02	0.08
P_1		1	-0.03	0.02	-0.08	0.03	0.03	0.08
P_2			1	0.04	-0.12	-0.14	-0.03	-0.05
P_3				1	-0.02	-0.02	-0.05	0.09
P'_4					1	-0.11	-0.01	-0.10
P'_5						1	-0.04	0.07
P'_6							1	0.05
P'_8								1

Table 17: Correlation matrix for the CP -averaged observables F_L and $P_i^{(\prime)}$ from the maximum-likelihood fit in the interval $6.0 < q^2 < 8.0 \text{ GeV}^2/c^4$.

	F_L	P_1	P_2	P_3	P'_4	P'_5	P'_6	P'_8
F_L	1	0.11	-0.10	0.01	-0.03	0.05	-0.05	-0.00
P_1		1	-0.04	0.01	0.01	-0.02	0.02	-0.06
P_2			1	0.12	-0.01	0.02	-0.05	-0.17
P_3				1	0.04	0.12	0.00	-0.04
P'_4					1	0.25	-0.03	-0.01
P'_5						1	-0.08	-0.06
P'_6							1	-0.05
P'_8								1

Table 18: Correlation matrix for the CP -averaged observables F_L and $P_i^{(\prime)}$ from the maximum-likelihood fit in the interval $11.0 < q^2 < 12.5 \text{ GeV}^2/c^4$.

	F_L	P_1	P_2	P_3	P'_4	P'_5	P'_6	P'_8
F_L	1	-0.05	0.35	-0.09	0.00	0.04	-0.06	-0.14
P_1		1	-0.05	0.17	-0.09	-0.14	-0.03	-0.02
P_2			1	-0.15	0.12	-0.14	-0.00	0.07
P_3				1	-0.09	0.06	0.07	0.09
P'_4					1	0.04	-0.03	-0.10
P'_5						1	0.05	-0.01
P'_6							1	0.06
P'_8								1

Table 19: Correlation matrix for the CP -averaged observables F_L and $P_i^{(\prime)}$ from the maximum-likelihood fit in the interval $15.0 < q^2 < 17.0 \text{ GeV}^2/c^4$.

	F_L	P_1	P_2	P_3	P'_4	P'_5	P'_6	P'_8
F_L	1	0.07	0.15	-0.09	0.08	0.09	0.00	-0.09
P_1		1	0.01	-0.05	0.00	-0.01	-0.00	-0.06
P_2			1	-0.23	0.10	-0.06	0.07	-0.03
P_3				1	-0.15	0.10	-0.03	0.02
P'_4					1	0.27	0.09	0.05
P'_5						1	0.09	-0.07
P'_6							1	0.21
P'_8								1

Table 20: Correlation matrix for the CP -averaged observables F_L and $P_i^{(\prime)}$ from the maximum-likelihood fit in the interval $17.0 < q^2 < 19.0 \text{ GeV}^2/c^4$.

	F_L	P_1	P_2	P_3	P'_4	P'_5	P'_6	P'_8
F_L	1	-0.10	0.09	0.07	0.02	-0.10	0.06	-0.08
P_1		1	0.06	0.04	-0.10	0.02	-0.01	0.06
P_2			1	0.07	-0.07	-0.16	0.13	-0.00
P_3				1	-0.08	0.03	-0.08	0.17
P'_4					1	-0.08	-0.03	0.05
P'_5						1	0.00	0.08
P'_6							1	-0.12
P'_8								1

Table 21: Correlation matrix for the CP -averaged observables F_L and $P_i^{(\prime)}$ from the maximum-likelihood fit in the interval $1.1 < q^2 < 6.0 \text{ GeV}^2/c^4$.

	F_L	P_1	P_2	P_3	P'_4	P'_5	P'_6	P'_8
F_L	1	0.11	-0.19	0.01	-0.01	-0.02	0.02	0.08
P_1		1	-0.05	0.07	0.01	-0.01	0.00	-0.04
P_2			1	-0.06	0.04	0.00	-0.05	0.01
P_3				1	0.01	-0.04	0.01	0.01
P'_4					1	-0.03	-0.02	0.18
P'_5						1	0.14	0.04
P'_6							1	0.17
P'_8								1

Table 22: Correlation matrix for the CP -averaged observables F_L and $P_i^{(\prime)}$ from the maximum-likelihood fit in the interval $15.0 < q^2 < 19.0 \text{ GeV}^2/c^4$.

	F_L	P_1	P_2	P_3	P'_4	P'_5	P'_6	P'_8
F_L	1	-0.00	0.03	-0.01	0.00	0.01	0.03	0.05
P_1		1	0.01	0.04	-0.06	0.04	0.03	0.08
P_2			1	-0.07	-0.13	-0.00	-0.12	-0.03
P_3				1	0.03	0.04	0.02	0.08
P'_4					1	-0.00	0.12	0.04
P'_5						1	-0.09	0.07
P'_6							1	0.17
P'_8								1

5 Systematic uncertainties

The systematic uncertainties are determined for each observable in each q^2 interval. Table 23 summarises the sizes of the systematic effects by giving the maximum value for each systematic uncertainty studied.

The larger systematic uncertainties of the $P_i^{(\prime)}$ observables compared to the S_i observables arise due to an additional scale factor in the definition of the $P_i^{(\prime)}$ observables, which depends on the value of F_L for a given q^2 interval.

Table 23: Maximum values for each source of systematic uncertainty.

Source	F_L	A_{FB}	S_3-S_9	P_1	$P_2-P'_8$
Size of the simulation sample	< 0.03	< 0.03	< 0.04	< 0.06	< 0.08
Data-simulation differences	< 0.04	< 0.01	< 0.04	< 0.13	< 0.17
Acceptance polynomial order	< 0.05	< 0.04	< 0.06	< 0.09	< 0.10
S-wave fraction constraint	< 0.05	< 0.02	< 0.03	< 0.13	< 0.14
$m(K_S^0\pi^+\mu^+\mu^-)$ model	< 0.01	< 0.01	< 0.01	< 0.06	< 0.02
Peaking background veto	< 0.01	< 0.01	< 0.01	< 0.07	< 0.04
Angular resolution	< 0.01	< 0.01	< 0.01	< 0.01	< 0.01
Background model	< 0.01	< 0.01	< 0.02	< 0.06	< 0.12
Trigger simulation	< 0.01	< 0.01	< 0.01	< 0.03	< 0.03
Fit bias at best-fit values	< 0.04	< 0.05	< 0.05	< 0.28	< 0.13

6 Yields of signal candidates per q^2 interval

Table 24: Yields of signal candidates in the ten q^2 intervals. They are obtained from extended maximum-likelihood fits to the $m(K_S^0 \pi^+ \mu^+ \mu^-)$ distribution. The total number corresponds to the sum of the eight nominal q^2 intervals.

q^2 [GeV ² /c ⁴]	Signal yield
[0.1, 0.98]	102 ± 12
[1.1, 2.5]	49 ± 10
[2.5, 4.0]	42 ± 10
[4.0, 6.0]	109 ± 13
[6.0, 8.0]	105 ± 14
[11.0, 12.5]	111 ± 13
[15.0, 17.0]	144 ± 13
[17.0, 19.0]	76 ± 10
[1.1, 6.0]	200 ± 19
[15.0, 19.0]	220 ± 17
Total	737 ± 34

7 Projections of data and fit model

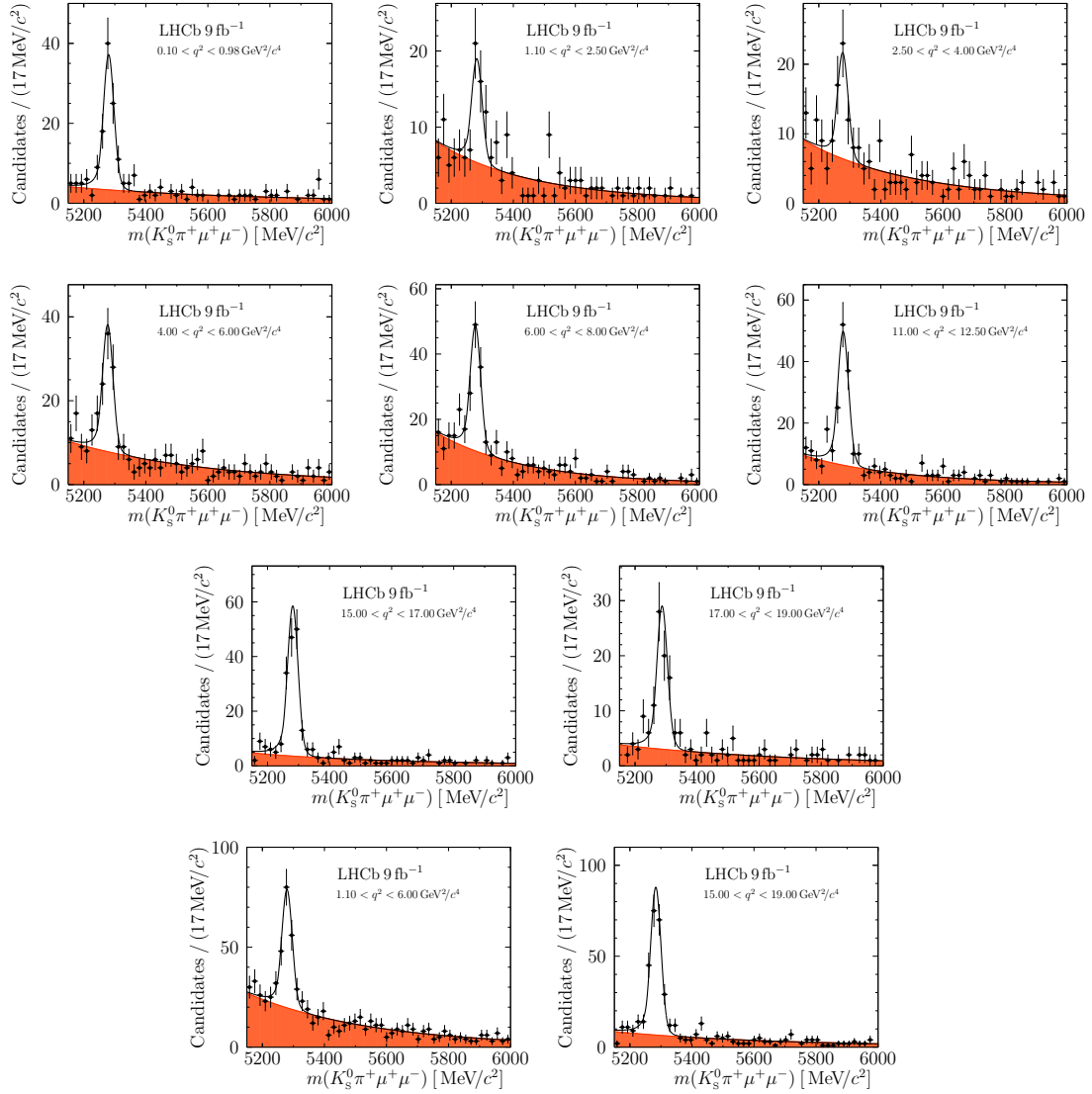


Figure 5: Projections for the invariant mass $m(K_S^0\pi^+\mu^+\mu^-)$ in the ten q^2 intervals. The black points represent the data, while the solid curve shows the fit result. The background component is represented by the orange shaded area.

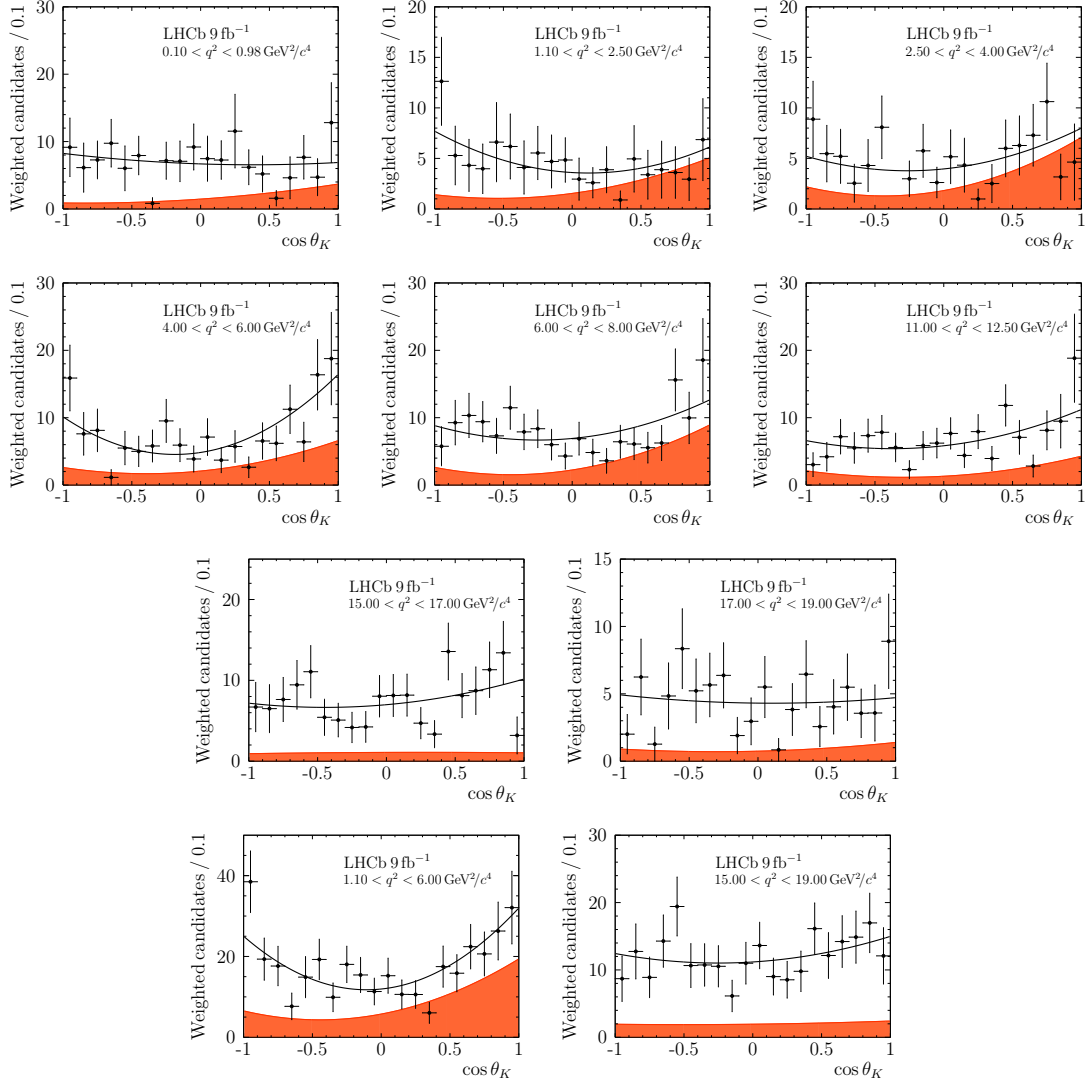


Figure 6: Projections for the angle $\cos \theta_K$ in the ten q^2 intervals. The black points represent the data, while the solid curve shows the fit result. The background component is represented by the orange shaded area. The invariant mass $m(K_S^0 \pi^+ \mu^+ \mu^-)$ is required to be within $50 \text{ MeV}/c^2$ of the measured B^+ meson mass.

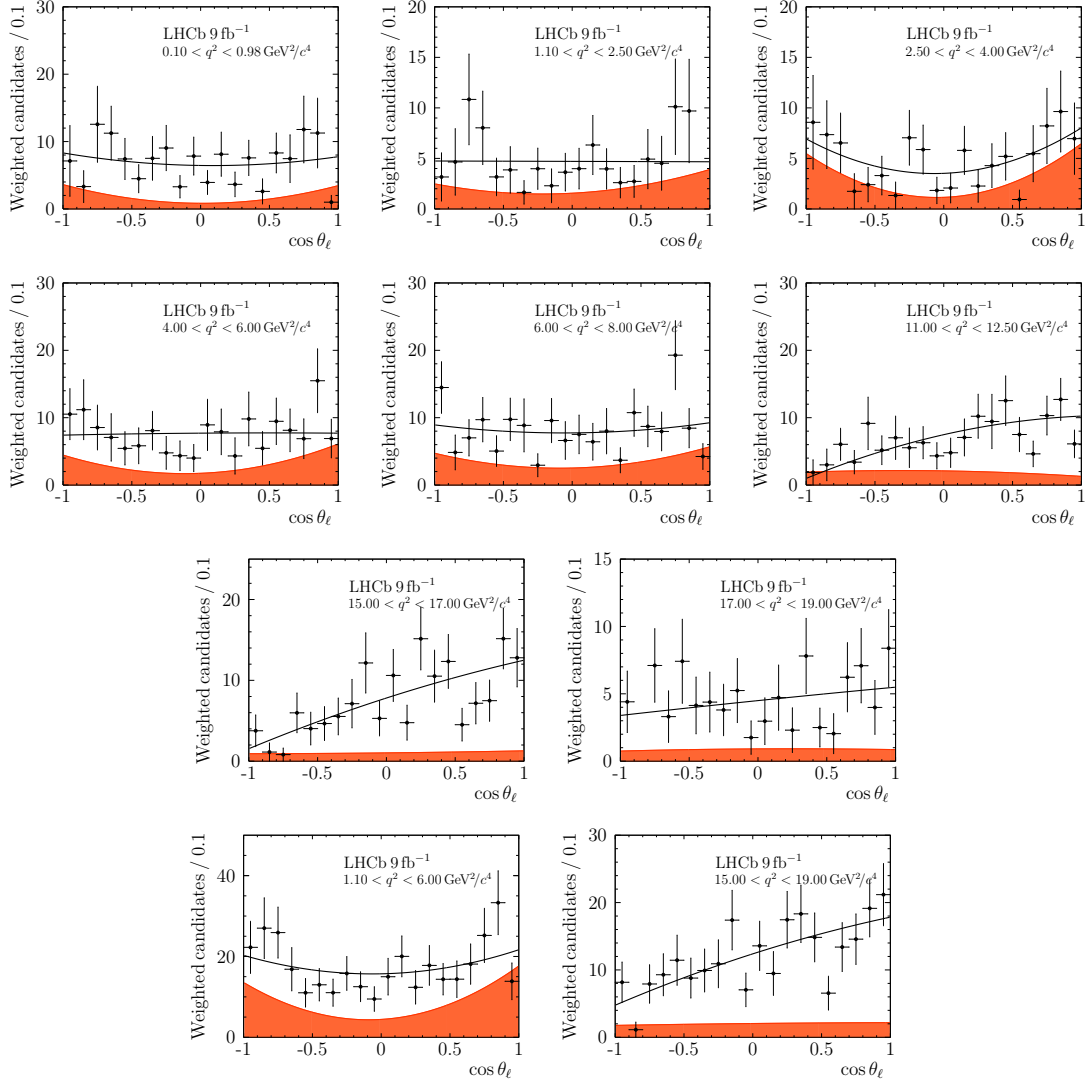


Figure 7: Projections for the angle $\cos\theta_\ell$ in the ten q^2 intervals. The black points represent the data, while the solid curve shows the fit result. The background component is represented by the orange shaded area. The invariant mass $m(K_S^0\pi^+\mu^+\mu^-)$ is required to be within $50 \text{ MeV}/c^2$ of the measured B^+ meson mass.

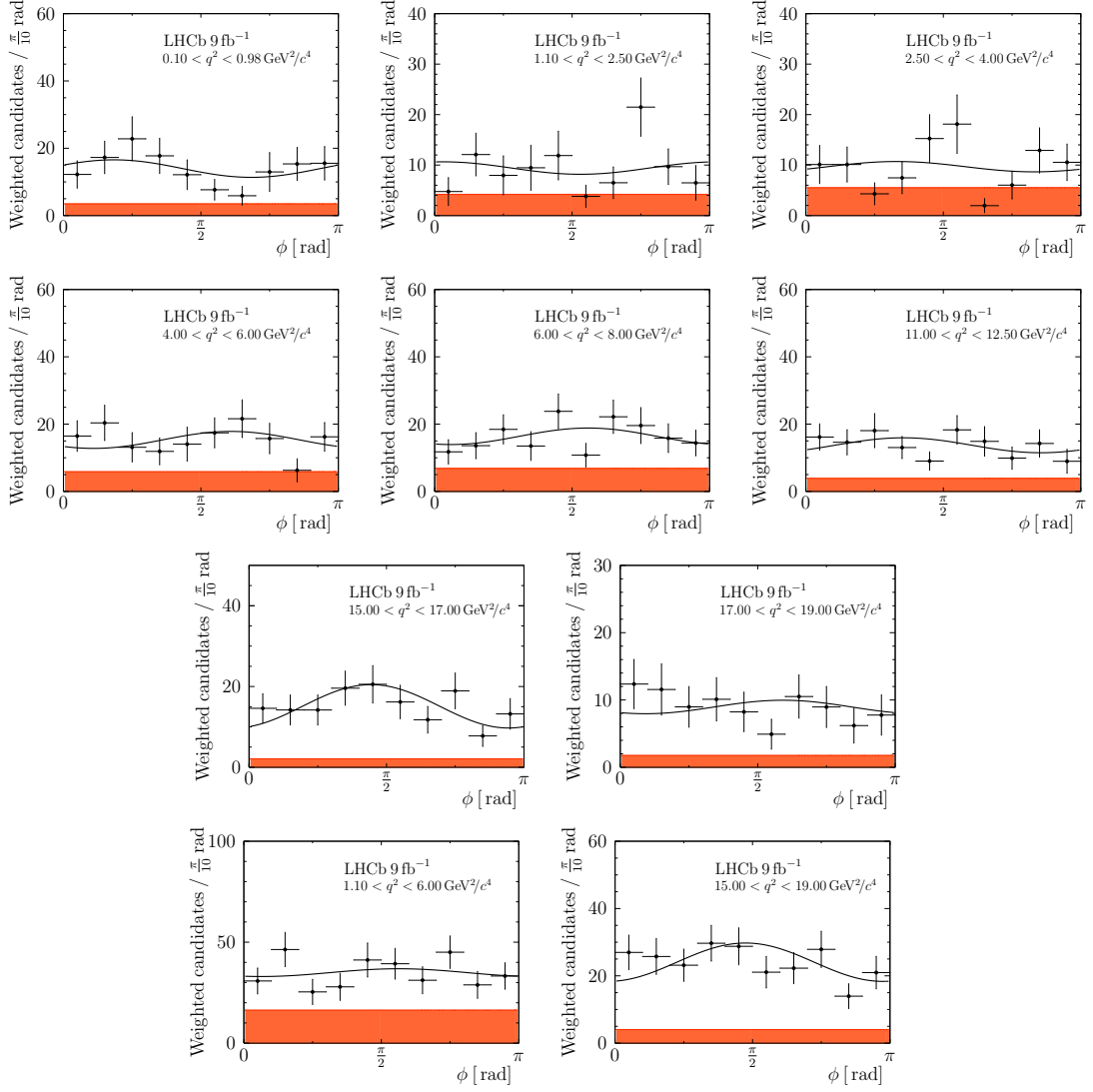


Figure 8: Projections for the angle ϕ in the ten q^2 intervals. The black points represent the data, while the solid curve shows the fit result. The background component is represented by the orange shaded area. The invariant mass $m(K_S^0\pi^+\mu^+\mu^-)$ is required to be within $50 \text{ MeV}/c^2$ of the measured B^+ meson mass.

References

- [1] BaBar collaboration, B. Aubert *et al.*, *Measurements of branching fractions, rate asymmetries, and angular distributions in the rare decays $B \rightarrow K\ell^+\ell^-$ and $B \rightarrow K^*\ell^+\ell^-$* , Phys. Rev. **D73** (2006) 092001, [arXiv:hep-ex/0604007](#).
- [2] LHCb collaboration, R. Aaij *et al.*, *Differential branching fractions and isospin asymmetries of $B \rightarrow K^{(*)}\mu^+\mu^-$ decays*, JHEP **06** (2014) 133, [arXiv:1403.8044](#).
- [3] LHCb collaboration, R. Aaij *et al.*, *Differential branching fraction and angular analysis of $\Lambda_b^0 \rightarrow \Lambda\mu^+\mu^-$ decays*, JHEP **06** (2015) 115, Erratum *ibid.* **09** (2018) 145, [arXiv:1503.07138](#).
- [4] LHCb collaboration, R. Aaij *et al.*, *Angular analysis and differential branching fraction of the decay $B_s^0 \rightarrow \phi\mu^+\mu^-$* , JHEP **09** (2015) 179, [arXiv:1506.08777](#).
- [5] LHCb collaboration, R. Aaij *et al.*, *Measurements of the S-wave fraction in $B^0 \rightarrow K^+\pi^-\mu^+\mu^-$ decays and the $B^0 \rightarrow K^*(892)^0\mu^+\mu^-$ differential branching fraction*, JHEP **11** (2016) 047, Erratum *ibid.* **04** (2017) 142, [arXiv:1606.04731](#).
- [6] CDF collaboration, T. Aaltonen *et al.*, *Measurements of the angular distributions in the decays $B \rightarrow K^{(*)}\mu^+\mu^-$ at CDF*, Phys. Rev. Lett. **108** (2012) 081807, [arXiv:1108.0695](#).
- [7] LHCb collaboration, R. Aaij *et al.*, *Angular analysis of the $B^0 \rightarrow K^{*0}\mu^+\mu^-$ decay using 3fb^{-1} of integrated luminosity*, JHEP **02** (2016) 104, [arXiv:1512.04442](#).
- [8] Belle collaboration, S. Wehle *et al.*, *Lepton-flavor-dependent angular analysis of $B \rightarrow K^*\ell^+\ell^-$* , Phys. Rev. Lett. **118** (2017) 111801, [arXiv:1612.05014](#).
- [9] CMS collaboration, A. M. Sirunyan *et al.*, *Measurement of angular parameters from the decay $B^0 \rightarrow K^{*0}\mu^+\mu^-$ in proton-proton collisions at $\sqrt{s} = 8\text{ TeV}$* , Phys. Lett. **B781** (2018) 517, [arXiv:1710.02846](#).
- [10] ATLAS collaboration, M. Aaboud *et al.*, *Angular analysis of $B_d^0 \rightarrow K^*\mu^+\mu^-$ decays in pp collisions at $\sqrt{s} = 8\text{ TeV}$ with the ATLAS detector*, JHEP **10** (2018) 047, [arXiv:1805.04000](#).
- [11] LHCb collaboration, R. Aaij *et al.*, *Angular moments of the decay $\Lambda_b^0 \rightarrow \Lambda\mu^+\mu^-$ at low hadronic recoil*, JHEP **09** (2018) 146, [arXiv:1808.00264](#).
- [12] LHCb collaboration, R. Aaij *et al.*, *Measurement of CP-averaged observables in the $B^0 \rightarrow K^{*0}\mu^+\mu^-$ decay*, Phys. Rev. Lett. **125** (2020) 011802, [arXiv:2003.04831](#).
- [13] CMS collaboration, A. M. Sirunyan *et al.*, *Angular analysis of the decay $B^+ \rightarrow K^*(892)^+\mu^+\mu^-$ in proton-proton collisions at $\sqrt{s} = 8\text{ TeV}$* , [arXiv:2010.13968](#).
- [14] BaBar collaboration, J. P. Lees *et al.*, *Measurement of branching fractions and rate asymmetries in the rare decays $B \rightarrow K^{(*)}\ell^+\ell^-$* , Phys. Rev. **D86** (2012) 032012, [arXiv:1204.3933](#).

- [15] LHCb collaboration, R. Aaij *et al.*, *Test of lepton universality with $B^0 \rightarrow K^{*0} \ell^+ \ell^-$ decays*, JHEP **08** (2017) 055, [arXiv:1705.05802](#).
- [16] LHCb collaboration, R. Aaij *et al.*, *Search for lepton-universality violation in $B^+ \rightarrow K^+ \ell^+ \ell^-$ decays*, Phys. Rev. Lett. **122** (2019) 191801, [arXiv:1903.09252](#).
- [17] Belle collaboration, S. Choudhury *et al.*, *Test of lepton flavor universality and search for lepton flavor violation in $B \rightarrow K \ell \ell$ decays*, [arXiv:1908.01848](#), submitted to JHEP.
- [18] Belle collaboration, S. Wehle *et al.*, *Test of lepton-flavor universality in $B \rightarrow K^* \ell^+ \ell^-$ decays at belle*, [arXiv:1904.02440](#), submitted to Phys. Rev. Lett.
- [19] W. Altmannshofer, S. Gori, M. Pospelov, and I. Yavin, *Quark flavor transitions in $L_\mu - L_\tau$ models*, Phys. Rev. **D89** (2014) 095033, [arXiv:1403.1269](#).
- [20] G. Hiller and M. Schmaltz, *R_K and future $b \rightarrow s \ell \ell$ physics beyond the standard model opportunities*, Phys. Rev. **D90** (2014) 054014, [arXiv:1408.1627](#).
- [21] B. Gripaios, M. Nardecchia, and S. A. Renner, *Composite leptoquarks and anomalies in B -meson decays*, JHEP **05** (2015) 006, [arXiv:1412.1791](#).
- [22] I. de Medeiros Varzielas and G. Hiller, *Clues for flavor from rare lepton and quark decays*, JHEP **06** (2015) 072, [arXiv:1503.01084](#).
- [23] A. Crivellin, G. D'Ambrosio, and J. Heeck, *Explaining $h \rightarrow \mu^\pm \tau^\mp$, $B \rightarrow K^* \mu^+ \mu^-$ and $B \rightarrow K \mu^+ \mu^- / B \rightarrow K e^+ e^-$ in a two-Higgs-doublet model with gauged $L_\mu - L_\tau$* , Phys. Rev. Lett. **114** (2015) 151801, [arXiv:1501.00993](#).
- [24] A. Celis, J. Fuentes-Martín, M. Jung, and H. Serôdio, *Family nonuniversal Z' models with protected flavor-changing interactions*, Phys. Rev. **D92** (2015) 015007, [arXiv:1505.03079](#).
- [25] A. Falkowski, M. Nardecchia, and R. Ziegler, *Lepton flavor non-universality in B -meson decays from a $U(2)$ flavor model*, JHEP **11** (2015) 173, [arXiv:1509.01249](#).
- [26] R. Barbieri, C. W. Murphy, and F. Senia, *B -decay anomalies in a composite leptoquark model*, Eur. Phys. J. **C77** (2017) 8, [arXiv:1611.04930](#).
- [27] A. Crivellin, D. Müller, and T. Ota, *Simultaneous explanation of $R(D^{(*)})$ and $b \rightarrow s \mu^+ \mu^-$: the last scalar leptoquarks standing*, JHEP **09** (2017) 040, [arXiv:1703.09226](#).
- [28] F. Sala and D. M. Straub, *A new light particle in B decays?*, Phys. Lett. **B774** (2017) 205, [arXiv:1704.06188](#).
- [29] P. Ko, Y. Omura, Y. Shigekami, and C. Yu, *LHCb anomaly and B physics in flavored Z' models with flavored Higgs doublets*, Phys. Rev. **D95** (2017) 115040, [arXiv:1702.08666](#).
- [30] J.-H. Sheng, R.-M. Wang, and Y.-D. Yang, *Scalar leptoquark effects in the lepton flavor violating exclusive $b \rightarrow s \ell_i^- \ell_j^+$ decays*, Int. J. Theor. Phys. **58** (2019) 480, [arXiv:1805.05059](#).

- [31] G. Hiller, D. Loose, and I. Nišandžić, *Flavorful leptoquarks at hadron colliders*, Phys. Rev. **D97** (2018) 075004, arXiv:1801.09399.
- [32] M. Algueró *et al.*, *Emerging patterns of new physics with and without Lepton flavour universal contributions*, Eur. Phys. J. **C79** (2019) 714, arXiv:1903.09578.
- [33] J. Aebischer *et al.*, *B-decay discrepancies after Moriond 2019*, Eur. Phys. J. **C80** (2020) 252, arXiv:1903.10434.
- [34] A. Arbey *et al.*, *Update on the $b \rightarrow s$ anomalies*, Phys. Rev. **D100** (2019) 015045, arXiv:1904.08399.
- [35] M. Ciuchini *et al.*, *New physics in $b \rightarrow s\ell^+\ell^-$ confronts new data on lepton universality*, Eur. Phys. J. **C79** (2019) 719, arXiv:1903.09632.
- [36] K. Kowalska, D. Kumar, and E. M. Sessolo, *Implications for new physics in $b \rightarrow s\mu\mu$ transitions after recent measurements by Belle and LHCb*, Eur. Phys. J. **C79** (2019) 840, arXiv:1903.10932.
- [37] A. K. Alok, A. Dighe, S. Gangal, and D. Kumar, *Continuing search for new physics in $b \rightarrow s\mu\mu$ decays: Two operators at a time*, JHEP **06** (2019) 089, arXiv:1903.09617.
- [38] S. Jäger and J. Martin Camalich, *Reassessing the discovery potential of the $B \rightarrow K^*\ell^+\ell^-$ decays in the large-recoil region: SM challenges and BSM opportunities*, Phys. Rev. **D93** (2016) 014028, arXiv:1412.3183.
- [39] J. Lyon and R. Zwicky, *Resonances gone topsy turvy - the charm of QCD or new physics in $b \rightarrow s\ell^+\ell^-$?*, arXiv:1406.0566.
- [40] M. Ciuchini *et al.*, *$B \rightarrow K^*\ell^+\ell^-$ decays at large recoil in the Standard Model: a theoretical reappraisal*, JHEP **06** (2016) 116, arXiv:1512.07157.
- [41] C. Bobeth, M. Chrzaszcz, D. van Dyk, and J. Virto, *Long-distance effects in $B \rightarrow K^*\ell\ell$ from analyticity*, Eur. Phys. J. **C78** (2018) 451, arXiv:1707.07305.
- [42] N. Gubernari, D. van Dyk, and J. Virto, *Non-local matrix elements in $B_{(s)} \rightarrow \{K^{(*)}, \phi\}\ell^+\ell^-$* , JHEP **02** (2021) 088, arXiv:2011.09813.
- [43] LHCb collaboration, R. Aaij *et al.*, *Measurement of form-factor-independent observables in the decay $B^0 \rightarrow K^{*0}\mu^+\mu^-$* , Phys. Rev. Lett. **111** (2013) 191801, arXiv:1308.1707.
- [44] LHCb collaboration, R. Aaij *et al.*, *Differential branching fraction and angular analysis of the decay $B^0 \rightarrow K^{*0}\mu^+\mu^-$* , JHEP **08** (2013) 131, arXiv:1304.6325.
- [45] P. Ball, G. W. Jones, and R. Zwicky, *$B \rightarrow V\gamma$ beyond QCD factorization*, Phys. Rev. **D75** (2007) 054004, arXiv:hep-ph/0612081v3.
- [46] Belle collaboration, T. Horiguchi *et al.*, *Evidence for Isospin Violation and Measurement of CP Asymmetries in $B \rightarrow K^*(892)\gamma$* , Phys. Rev. Lett. **119** (2017) 191802, arXiv:1707.00394.

- [47] LHCb collaboration, A. A. Alves Jr. *et al.*, *The LHCb detector at the LHC*, JINST **3** (2008) S08005.
- [48] LHCb collaboration, R. Aaij *et al.*, *LHCb detector performance*, Int. J. Mod. Phys. **A30** (2015) 1530022, arXiv:1412.6352.
- [49] R. Aaij *et al.*, *Performance of the LHCb Vertex Locator*, JINST **9** (2014) P09007, arXiv:1405.7808.
- [50] R. Arink *et al.*, *Performance of the LHCb Outer Tracker*, JINST **9** (2014) P01002, arXiv:1311.3893.
- [51] P. d'Argent *et al.*, *Improved performance of the LHCb Outer Tracker in LHC Run 2*, JINST **12** (2017) P11016, arXiv:1708.00819.
- [52] M. Adinolfi *et al.*, *Performance of the LHCb RICH detector at the LHC*, Eur. Phys. J. **C73** (2013) 2431, arXiv:1211.6759.
- [53] A. A. Alves Jr. *et al.*, *Performance of the LHCb muon system*, JINST **8** (2013) P02022, arXiv:1211.1346.
- [54] R. Aaij *et al.*, *The LHCb trigger and its performance in 2011*, JINST **8** (2013) P04022, arXiv:1211.3055.
- [55] R. Aaij *et al.*, *Performance of the LHCb trigger and full real-time reconstruction in Run 2 of the LHC*, JINST **14** (2019) P04013, arXiv:1812.10790.
- [56] T. Sjöstrand, S. Mrenna, and P. Skands, *A brief introduction to PYTHIA 8.1*, Comput. Phys. Commun. **178** (2008) 852, arXiv:0710.3820; T. Sjöstrand, S. Mrenna, and P. Skands, *PYTHIA 6.4 physics and manual*, JHEP **05** (2006) 026, arXiv:hep-ph/0603175.
- [57] I. Belyaev *et al.*, *Handling of the generation of primary events in Gauss, the LHCb simulation framework*, J. Phys. Conf. Ser. **331** (2011) 032047.
- [58] D. J. Lange, *The EvtGen particle decay simulation package*, Nucl. Instrum. Meth. **A462** (2001) 152.
- [59] P. Golonka and Z. Was, *PHOTOS Monte Carlo: A precision tool for QED corrections in Z and W decays*, Eur. Phys. J. **C45** (2006) 97, arXiv:hep-ph/0506026.
- [60] Geant4 collaboration, J. Allison *et al.*, *Geant4 developments and applications*, IEEE Trans. Nucl. Sci. **53** (2006) 270; Geant4 collaboration, S. Agostinelli *et al.*, *Geant4: A simulation toolkit*, Nucl. Instrum. Meth. **A506** (2003) 250.
- [61] M. Clemencic *et al.*, *The LHCb simulation application, Gauss: Design, evolution and experience*, J. Phys. Conf. Ser. **331** (2011) 032023.
- [62] Particle Data Group, P. A. Zyla *et al.*, *Review of Particle Physics*, PTEP **2020** (2020) 083C01.
- [63] W. D. Hulsbergen, *Decay chain fitting with a Kalman filter*, Nucl. Instrum. Meth. **A552** (2005) 566, arXiv:physics/0503191.

- [64] L. Breiman, J. H. Friedman, R. A. Olshen, and C. J. Stone, *Classification and regression trees*, Wadsworth international group, Belmont, California, USA, 1984.
- [65] Y. Freund and R. E. Schapire, *A decision-theoretic generalization of on-line learning and an application to boosting*, J. Comput. Syst. Sci. **55** (1997) 119.
- [66] H. Voss, A. Hoecker, J. Stelzer, and F. Tegenfeldt, *TMVA - Toolkit for Multivariate Data Analysis with ROOT*, PoS **ACAT** (2007) 040.
- [67] LHCb collaboration, R. Aaij *et al.*, *Measurement of the branching fraction and CP asymmetry in $B^+ \rightarrow J/\psi \rho^+$ decays*, Eur. Phys. J. **C79** (2019) 537, [arXiv:1812.07041](#).
- [68] S. Descotes-Genon, J. Matias, M. Ramon, and J. Virto, *Implications from clean observables for the binned analysis of $B \rightarrow K^* \mu^+ \mu^-$ at large recoil*, JHEP **01** (2013) 048, [arXiv:1207.2753](#).
- [69] M. De Cian, *Track Reconstruction Efficiency and Analysis of $B^0 \rightarrow K^{*0} \mu^+ \mu^-$ at the LHCb Experiment*, PhD thesis, University of Zurich, 2013, CERN-THESIS-2013-145.
- [70] D. Aston *et al.*, *A Study of $K^- \pi^+$ scattering in the reaction $K^- \pi^+ \rightarrow K^- \pi^+ n$ at 11 GeV/c*, Nucl. Phys. **B296** (1988) 493.
- [71] B. Efron, *Bootstrap methods: Another look at the jackknife*, Ann. Statist. **7** (1979) 1.
- [72] G. J. Feldman and R. D. Cousins, *Unified approach to the classical statistical analysis of small signals*, Phys. Rev. **D57** (1998) 3873, [arXiv:physics/9711021](#).
- [73] BaBar collaboration, B. Aubert *et al.*, *Measurement of decay amplitudes of $B \rightarrow J/\psi K^*$, $\psi(2S) K^*$, and $\chi_{c1} K^*$ with an angular analysis*, Phys. Rev. **D76** (2007) 031102, [arXiv:0704.0522](#).
- [74] Belle collaboration, R. Itoh *et al.*, *Studies of CP violation in $B \rightarrow J/\psi K^*$ decays*, Phys. Rev. Lett. **95** (2005) 091601, [arXiv:hep-ex/0504030](#).
- [75] LHCb collaboration, R. Aaij *et al.*, *Measurement of the polarization amplitudes in $B^0 \rightarrow J/\psi K^*(892)^0$ decays*, Phys. Rev. **D88** (2013) 052002, [arXiv:1307.2782](#).
- [76] W. Altmannshofer and D. M. Straub, *New physics in $b \rightarrow s$ transitions after LHC run 1*, Eur. Phys. J. **C75** (2015) 382, [arXiv:1411.3161](#).
- [77] A. Bharucha, D. M. Straub, and R. Zwicky, *$B \rightarrow V \ell^+ \ell^-$ in the Standard Model from light-cone sum rules*, JHEP **08** (2016) 098, [arXiv:1503.05534](#).
- [78] R. R. Horgan, Z. Liu, S. Meinel, and M. Wingate, *Lattice QCD calculation of form factors describing the rare decays $B \rightarrow K^* \ell^+ \ell^-$ and $B_s \rightarrow \phi \ell^+ \ell^-$* , Phys. Rev. **D89** (2014) 094501, [arXiv:1310.3722](#).
- [79] R. R. Horgan, Z. Liu, S. Meinel, and M. Wingate, *Rare B decays using lattice QCD form factors*, PoS LATTICE2014 (2015) 372, [arXiv:1501.00367](#).
- [80] S. Descotes-Genon, L. Hofer, J. Matias, and J. Virto, *Global analysis of $b \rightarrow s \ell \ell$ anomalies*, JHEP **06** (2016) 92, [arXiv:1510.04239](#).

- [81] B. Capdevila *et al.*, *Patterns of new physics in $b \rightarrow sl^+\ell^-$ transitions in the light of recent data*, JHEP **01** (2018) 93, [arXiv:1704.05340](#).
- [82] A. Khodjamirian, T. Mannel, A. A. Pivovarov, and Y.-M. Wang, *Charm-loop effect in $B \rightarrow K^{(*)}\ell^+\ell^-$ and $B \rightarrow K^*\gamma$* , JHEP **09** (2010) 089, [arXiv:1006.4945](#).
- [83] D. M. Straub, *FLAVIO: A python package for flavour and precision phenomenology in the Standard Model and beyond*, [arXiv:1810.08132](#).
- [84] B. Grinstein and D. Pirjol, *Exclusive rare $B \rightarrow K^*\ell^+\ell^-$ decays at low recoil: Controlling the long-distance effects*, Phys. Rev. **D70** (2004) 114005, [arXiv:hep-ph/0404250](#).
- [85] M. Beylich, G. Buchalla, and T. Feldmann, *Theory of $B \rightarrow K^{(*)}\ell^+\ell^-$ decays at high q^2 : OPE and quark-hadron duality*, Eur. Phys. J. **C71** (2011) 1635, [arXiv:1101.5118](#).
- [86] S. Braß, G. Hiller, and I. Nisandzic, *Zooming in on $B \rightarrow K^*\ell\ell$ decays at low recoil*, Eur. Phys. J. **C77** (2017) 16, [arXiv:1606.00775](#).

LHCb collaboration

R. Aaij³², C. Abellán Beteta⁵⁰, T. Ackernley⁶⁰, B. Adeva⁴⁶, M. Adinolfi⁵⁴, H. Afsharnia⁹, C.A. Aidala⁸⁵, S. Aiola²⁶, Z. Ajaltouni⁹, S. Akar⁶⁵, J. Albrecht¹⁵, F. Alessio⁴⁸, M. Alexander⁵⁹, A. Alfonso Alberio⁴⁵, Z. Aliouche⁶², G. Alkhazov³⁸, P. Alvarez Cartelle⁵⁵, S. Amato², Y. Amhis¹¹, L. An⁴⁸, L. Anderlini²², A. Andreianov³⁸, M. Andreotti²¹, F. Archilli¹⁷, A. Artamonov⁴⁴, M. Artuso⁶⁸, K. Arzymatov⁴², E. Aslanides¹⁰, M. Atzeni⁵⁰, B. Audurier¹², S. Bachmann¹⁷, M. Bachmayer⁴⁹, J.J. Back⁵⁶, S. Baker⁶¹, P. Baladron Rodriguez⁴⁶, V. Balagura¹², W. Baldini²¹, J. Baptista Leite¹, R.J. Barlow⁶², S. Barsuk¹¹, W. Barter⁶¹, M. Bartolini^{24,h}, F. Baryshnikov⁸¹, J.M. Basels¹⁴, G. Bassi²⁹, B. Batsukh⁶⁸, A. Battig¹⁵, A. Bay⁴⁹, M. Becker¹⁵, F. Bedeschi²⁹, I. Bediaga¹, A. Beiter⁶⁸, V. Belavin⁴², S. Belin²⁷, V. Bellee⁴⁹, K. Belous⁴⁴, I. Belov⁴⁰, I. Belyaev³⁹, G. Bencivenni²³, E. Ben-Haim¹³, A. Berezhnoy⁴⁰, R. Bernet⁵⁰, D. Berninghoff¹⁷, H.C. Bernstein⁶⁸, C. Bertella⁴⁸, A. Bertolin²⁸, C. Betancourt⁵⁰, F. Betti^{20,d}, Ia. Bezshyiko⁵⁰, S. Bhasin⁵⁴, J. Bhom³⁴, L. Bian⁷³, M.S. Bieker¹⁵, S. Bifani⁵³, P. Billoir¹³, M. Birch⁶¹, F.C.R. Bishop⁵⁵, A. Bizzeti^{22,r}, M. Bjørn⁶³, M.P. Blago⁴⁸, T. Blake⁵⁶, F. Blanc⁴⁹, S. Blusk⁶⁸, D. Bobulska⁵⁹, J.A. Boelhauve¹⁵, O. Boente Garcia⁴⁶, T. Boettcher⁶⁴, A. Boldyrev⁸², A. Bondar⁴³, N. Bondar³⁸, S. Borghi⁶², M. Borisyak⁴², M. Borsato¹⁷, J.T. Borsuk³⁴, S.A. Bouchiba⁴⁹, T.J.V. Bowcock⁶⁰, A. Boyer⁴⁸, C. Bozzi²¹, M.J. Bradley⁶¹, S. Braun⁶⁶, A. Brea Rodriguez⁴⁶, M. Brodski⁴⁸, J. Brodzicka³⁴, A. Brossa Gonzalo⁵⁶, D. Brundu²⁷, A. Buonauro⁵⁰, C. Burr⁴⁸, A. Bursche²⁷, A. Butkevich⁴¹, J.S. Butter³², J. Buytaert⁴⁸, W. Byczynski⁴⁸, S. Cadeddu²⁷, H. Cai⁷³, R. Calabrese^{21,f}, L. Calefice^{15,13}, L. Calero Diaz²³, S. Cali²³, R. Calladine⁵³, M. Calvi^{25,i}, M. Calvo Gomez⁸⁴, P. Camargo Magalhaes⁵⁴, A. Camboni⁴⁵, P. Campana²³, A.F. Campoverde Quezada⁵, S. Capelli^{25,i}, L. Capriotti^{20,d}, A. Carbone^{20,d}, G. Carboni³⁰, R. Cardinale^{24,h}, A. Cardini²⁷, I. Carli⁶, P. Carniti^{25,i}, K. Carvalho Akiba³², A. Casais Vidal⁴⁶, G. Casse⁶⁰, M. Cattaneo⁴⁸, G. Cavallero⁴⁸, S. Celani⁴⁹, J. Cerasoli¹⁰, A.J. Chadwick⁶⁰, M.G. Chapman⁵⁴, M. Charles¹³, Ph. Charpentier⁴⁸, G. Chatzikonstantinidis⁵³, C.A. Chavez Barajas⁶⁰, M. Chefdeville⁸, C. Chen³, S. Chen²⁷, A. Chernov³⁴, S.-G. Chitic⁴⁸, V. Chobanova⁴⁶, S. Cholak⁴⁹, M. Chruszcz³⁴, A. Chubykin³⁸, V. Chulikov³⁸, P. Ciambone²³, M.F. Cicala⁵⁶, X. Cid Vidal⁴⁶, G. Ciezarek⁴⁸, P.E.L. Clarke⁵⁸, M. Clemencic⁴⁸, H.V. Cliff⁵⁵, J. Closier⁴⁸, J.L. Cobbedick⁶², V. Coco⁴⁸, J.A.B. Coelho¹¹, J. Cogan¹⁰, E. Cogneras⁹, L. Cojocariu³⁷, P. Collins⁴⁸, T. Colombo⁴⁸, L. Congedo^{19,c}, A. Contu²⁷, N. Cooke⁵³, G. Coombs⁵⁹, G. Corti⁴⁸, C.M. Costa Sobral⁵⁶, B. Couturier⁴⁸, D.C. Craik⁶⁴, J. Crkovašá⁶⁷, M. Cruz Torres¹, R. Currie⁵⁸, C.L. Da Silva⁶⁷, E. Dall'Occo¹⁵, J. Dalseno⁴⁶, C. D'Ambrosio⁴⁸, A. Danilina³⁹, P. d'Argent⁴⁸, A. Davis⁶², O. De Aguiar Francisco⁶², K. De Bruyn⁷⁸, S. De Capua⁶², M. De Cian⁴⁹, J.M. De Miranda¹, L. De Paula², M. De Serio^{19,c}, D. De Simone⁵⁰, P. De Simone²³, J.A. de Vries⁷⁹, C.T. Dean⁶⁷, W. Dean⁸⁵, D. Decamp⁸, L. Del Buono¹³, B. Delaney⁵⁵, H.-P. Dembinski¹⁵, A. Dendek³⁵, V. Denysenko⁵⁰, D. Derkach⁸², O. Deschamps⁹, F. Desse¹¹, F. Dettori^{27,e}, B. Dey⁷³, P. Di Nezza²³, S. Didenko⁸¹, L. Dieste Maronas⁴⁶, H. Dijkstra⁴⁸, V. Dobishuk⁵², A.M. Donohoe¹⁸, F. Dordei²⁷, A.C. dos Reis¹, L. Douglas⁵⁹, A. Dovbnya⁵¹, A.G. Downes⁸, K. Dreimaniš⁶⁰, M.W. Dudek³⁴, L. Dufour⁴⁸, V. Duk⁷⁷, P. Durante⁴⁸, J.M. Durham⁶⁷, D. Dutta⁶², M. Dziewiecki¹⁷, A. Dziurda³⁴, A. Dzyuba³⁸, S. Easo⁵⁷, U. Egede⁶⁹, V. Egorychev³⁹, S. Eidelman^{43,u}, S. Eisenhardt⁵⁸, S. Ek-In⁴⁹, L. Eklund^{59,v}, S. Ely⁶⁸, A. Ene³⁷, E. Epple⁶⁷, S. Escher¹⁴, J. Eschle⁵⁰, S. Esen³², T. Evans⁴⁸, A. Falabella²⁰, J. Fan³, Y. Fan⁵, B. Fang⁷³, N. Farley⁵³, S. Farry⁶⁰, D. Fazzini^{25,i}, P. Fedin³⁹, M. Féo⁴⁸, P. Fernandez Declara⁴⁸, A. Fernandez Prieto⁴⁶, J.M. Fernandez-tenllado Arribas⁴⁵, F. Ferrari^{20,d}, L. Ferreira Lopes⁴⁹, F. Ferreira Rodrigues², S. Ferreres Sole³², M. Ferrillo⁵⁰, M. Ferro-Luzzi⁴⁸, S. Filippov⁴¹, R.A. Fini¹⁹, M. Fiorini^{21,f}, M. Firlej³⁵, K.M. Fischer⁶³, C. Fitzpatrick⁶², T. Fiutowski³⁵, F. Fleuret¹², M. Fontana¹³, F. Fontanelli^{24,h}, R. Forty⁴⁸, V. Franco Lima⁶⁰, M. Franco Sevilla⁶⁶, M. Frank⁴⁸, E. Franzoso²¹, G. Frau¹⁷, C. Frei⁴⁸, D.A. Friday⁵⁹, J. Fu²⁶, Q. Fuehring¹⁵,

W. Funk⁴⁸, E. Gabriel³², T. Gaintseva⁴², A. Gallas Torreira⁴⁶, D. Galli^{20,d}, S. Gambetta^{58,48},
 Y. Gan³, M. Gandelman², P. Gandini²⁶, Y. Gao⁴, M. Garau²⁷, L.M. Garcia Martin⁵⁶,
 P. Garcia Moreno⁴⁵, J. García Pardiñas²⁵, B. Garcia Plana⁴⁶, F.A. Garcia Rosales¹²,
 L. Garrido⁴⁵, C. Gaspar⁴⁸, R.E. Geertsema³², D. Gerick¹⁷, L.L. Gerken¹⁵, E. Gersabeck⁶²,
 M. Gersabeck⁶², T. Gershon⁵⁶, D. Gerstel¹⁰, Ph. Ghez⁸, V. Gibson⁵⁵, M. Giovannetti^{23,j},
 A. Gioventù⁴⁶, P. Gironella Gironell⁴⁵, L. Giubega³⁷, C. Giugliano^{21,48,f}, K. Gizdov⁵⁸,
 E.L. Gkougkousis⁴⁸, V.V. Gligorov¹³, C. Göbel⁷⁰, E. Golobardes⁸⁴, D. Golubkov³⁹,
 A. Golutvin^{61,81}, A. Gomes^{1,a}, S. Gomez Fernandez⁴⁵, F. Goncalves Abrantes⁷⁰, M. Goncerz³⁴,
 G. Gong³, P. Gorbounov³⁹, I.V. Gorelov⁴⁰, C. Gotti^{25,i}, E. Govorkova⁴⁸, J.P. Grabowski¹⁷,
 R. Graciani Diaz⁴⁵, T. Grammatico¹³, L.A. Granado Cardoso⁴⁸, E. Graugés⁴⁵, E. Graverini⁴⁹,
 G. Graziani²², A. Grecu³⁷, L.M. Greeven³², P. Griffith²¹, L. Grillo⁶², S. Gromov⁸¹,
 B.R. Gruberg Cazon⁶³, C. Gu³, M. Guarise²¹, P. A. Günther¹⁷, E. Gushchin⁴¹, A. Guth¹⁴,
 Y. Guz^{44,48}, T. Gys⁴⁸, T. Hadavizadeh⁶⁹, G. Haefeli⁴⁹, C. Haen⁴⁸, J. Haimberger⁴⁸,
 T. Halewood-leagas⁶⁰, P.M. Hamilton⁶⁶, Q. Han⁷, X. Han¹⁷, T.H. Hancock⁶³,
 S. Hansmann-Menzemer¹⁷, N. Harnew⁶³, T. Harrison⁶⁰, C. Hasse⁴⁸, M. Hatch⁴⁸, J. He⁵,
 M. Hecker⁶¹, K. Heijhoff³², K. Heinicke¹⁵, A.M. Hennequin⁴⁸, K. Hennessy⁶⁰, L. Henry^{26,47},
 J. Heuel¹⁴, A. Hicheur², D. Hill⁴⁹, M. Hilton⁶², S.E. Hollitt¹⁵, J. Hu¹⁷, J. Hu⁷², W. Hu⁷,
 W. Huang⁵, X. Huang⁷³, W. Hulsbergen³², R.J. Hunter⁵⁶, M. Hushchyn⁸², D. Hutchcroft⁶⁰,
 D. Hynds³², P. Ibis¹⁵, M. Idzik³⁵, D. Ilin³⁸, P. Ilten⁶⁵, A. Inglese³⁸, A. Ishteev⁸¹, K. Ivshin³⁸,
 R. Jacobsson⁴⁸, S. Jakobsen⁴⁸, E. Jans³², B.K. Jashal⁴⁷, A. Jawahery⁶⁶, V. Jevtic¹⁵,
 M. Jezabek³⁴, F. Jiang³, M. John⁶³, D. Johnson⁴⁸, C.R. Jones⁵⁵, T.P. Jones⁵⁶, B. Jost⁴⁸,
 N. Jurik⁴⁸, S. Kandybei⁵¹, Y. Kang³, M. Karacson⁴⁸, N. Kazeev⁸², F. Keizer^{55,48}, M. Kenzie⁵⁶,
 T. Ketel³³, B. Khanji¹⁵, A. Kharisova⁸³, S. Kholodenko⁴⁴, K.E. Kim⁶⁸, T. Kirn¹⁴,
 V.S. Kirsebom⁴⁹, O. Kitouni⁶⁴, S. Klaver³², K. Klimaszewski³⁶, S. Koliiev⁵², A. Kondybayeva⁸¹,
 A. Konoplyannikov³⁹, P. Kopciewicz³⁵, R. Kopecna¹⁷, P. Koppenburg³², M. Korolev⁴⁰,
 I. Kostiuik^{32,52}, O. Kot⁵², S. Kotriakhova^{38,31}, P. Kravchenko³⁸, L. Kravchuk⁴¹,
 R.D. Krawczyk⁴⁸, M. Kreps⁵⁶, F. Kress⁶¹, S. Kretzschmar¹⁴, P. Krokovny^{43,u}, W. Krupa³⁵,
 W. Krzemien³⁶, W. Kucewicz^{34,k}, M. Kucharczyk³⁴, V. Kudryavtsev^{43,u}, H.S. Kuindersma³²,
 G.J. Kunde⁶⁷, T. Kvaratskheliya³⁹, D. Lacarrere⁴⁸, G. Lafferty⁶², A. Lai²⁷, A. Lampis²⁷,
 D. Lancierini⁵⁰, J.J. Lane⁶², R. Lane⁵⁴, G. Lanfranchi²³, C. Langenbruch¹⁴, J. Langer¹⁵,
 O. Lantwin^{50,81}, T. Latham⁵⁶, F. Lazzari^{29,s}, R. Le Gac¹⁰, S.H. Lee⁸⁵, R. Lefèvre⁹, A. Leflat⁴⁰,
 S. Legotin⁸¹, O. Leroy¹⁰, T. Lesiak³⁴, B. Leverington¹⁷, H. Li⁷², L. Li⁶³, P. Li¹⁷, Y. Li⁶, Y. Li⁶,
 Z. Li⁶⁸, X. Liang⁶⁸, T. Lin⁶¹, R. Lindner⁴⁸, V. Lisovskyi¹⁵, R. Litvinov²⁷, G. Liu⁷², H. Liu⁵,
 S. Liu⁶, X. Liu³, A. Loi²⁷, J. Lomba Castro⁴⁶, I. Longstaff⁵⁹, J.H. Lopes², G. Loustau⁵⁰,
 G.H. Lovell⁵⁵, Y. Lu⁶, D. Lucchesi^{28,l}, S. Luchuk⁴¹, M. Lucio Martinez³², V. Lukashenko³²,
 Y. Luo³, A. Lupato⁶², E. Luppi^{21,f}, O. Lupton⁵⁶, A. Lusiani^{29,q}, X. Lyu⁵, L. Ma⁶,
 S. Maccolini^{20,d}, F. Machefert¹¹, F. Maciuc³⁷, V. Macko⁴⁹, P. Mackowiak¹⁵,
 S. Maddrell-Mander⁵⁴, O. Madejczyk³⁵, L.R. Madhan Mohan⁵⁴, O. Maev³⁸, A. Maevskiy⁸²,
 D. Maisuzenko³⁸, M.W. Majewski³⁵, S. Malde⁶³, B. Malecki⁴⁸, A. Malinin⁸⁰, T. Maltsev^{43,u},
 H. Malygina¹⁷, G. Manca^{27,e}, G. Mancinelli¹⁰, R. Manera Escalero⁴⁵, D. Manuzzi^{20,d},
 D. Marangotto^{26,n}, J. Maratas^{9,t}, J.F. Marchand⁸, U. Marconi²⁰, S. Mariani^{22,48,g},
 C. Marin Benito¹¹, M. Marinangeli⁴⁹, P. Marino⁴⁹, J. Marks¹⁷, P.J. Marshall⁶⁰, G. Martellotti³¹,
 L. Martinazzoli^{48,i}, M. Martinelli^{25,i}, D. Martinez Santos⁴⁶, F. Martinez Vidal⁴⁷, A. Massafferri¹,
 M. Materok¹⁴, R. Matev⁴⁸, A. Mathad⁵⁰, Z. Mathe⁴⁸, V. Matiunin³⁹, C. Matteuzzi²⁵,
 K.R. Mattioli⁸⁵, A. Mauri³², E. Maurice¹², J. Mauricio⁴⁵, M. Mazurek³⁶, M. McCann⁶¹,
 L. McConnell¹⁸, T.H. Mcgrath⁶², A. McNab⁶², R. McNulty¹⁸, J.V. Mead⁶⁰, B. Meadows⁶⁵,
 C. Meaux¹⁰, G. Meier¹⁵, N. Meinert⁷⁶, D. Melnychuk³⁶, S. Meloni^{25,i}, M. Merk^{32,79}, A. Merli²⁶,
 L. Meyer Garcia², M. Mikhasenko⁴⁸, D.A. Milanese⁷⁴, E. Millard⁵⁶, M. Milovanovic⁴⁸,
 M.-N. Minard⁸, L. Minzoni^{21,f}, S.E. Mitchell⁵⁸, B. Mitreska⁶², D.S. Mitzel⁴⁸, A. Mödden¹⁵,
 R.A. Mohammed⁶³, R.D. Moise⁶¹, T. Mombächer¹⁵, I.A. Monroy⁷⁴, S. Monteil⁹, M. Morandin²⁸,

G. Morello²³, M.J. Morello^{29,q}, J. Moron³⁵, A.B. Morris⁷⁵, A.G. Morris⁵⁶, R. Mountain⁶⁸, H. Mu³, F. Muheim⁵⁸, M. Mukherjee⁷, M. Mulder⁴⁸, D. Müller⁴⁸, K. Müller⁵⁰, C.H. Murphy⁶³, D. Murray⁶², P. Muzzetto^{27,48}, P. Naik⁵⁴, T. Nakada⁴⁹, R. Nandakumar⁵⁷, T. Nanut⁴⁹, I. Nasteva², M. Needham⁵⁸, I. Neri^{21,f}, N. Neri^{26,n}, S. Neubert⁷⁵, N. Neufeld⁴⁸, R. Newcombe⁶¹, T.D. Nguyen⁴⁹, C. Nguyen-Mau⁴⁹, E.M. Niel¹¹, S. Nieswand¹⁴, N. Nikitin⁴⁰, N.S. Nolte⁴⁸, C. Nunez⁸⁵, A. Oblakowska-Mucha³⁵, V. Obraztsov⁴⁴, D.P. O'Hanlon⁵⁴, R. Oldeman^{27,e}, C.J.G. Onderwater⁷⁸, A. Ossowska³⁴, J.M. Ojalora Goicochea², T. Ovsiannikova³⁹, P. Owen⁵⁰, A. Oyanguren⁴⁷, B. Pagare⁵⁶, P.R. Pais⁴⁸, T. Pajero^{29,48,q}, A. Palano¹⁹, M. Palutan²³, Y. Pan⁶², G. Panshin⁸³, A. Papanestis⁵⁷, M. Pappagallo^{19,c}, L.L. Pappalardo^{21,f}, C. Pappenheimer⁶⁵, W. Parker⁶⁶, C. Parkes⁶², C.J. Parkinson⁴⁶, B. Passalacqua²¹, G. Passaleva²², A. Pastore¹⁹, M. Patel⁶¹, C. Patrignani^{20,d}, C.J. Pawley⁷⁹, A. Pearce⁴⁸, A. Pellegrino³², M. Pepe Altarelli⁴⁸, S. Perazzini²⁰, D. Pereima³⁹, P. Perret⁹, K. Petridis⁵⁴, A. Petrolini^{24,h}, A. Petrov⁸⁰, S. Petrucci⁵⁸, M. Petruzzo²⁶, A. Philippov⁴², L. Pica²⁹, M. Piccini⁷⁷, B. Pietrzyk⁸, G. Pietrzyk⁴⁹, M. Pili⁶³, D. Pinci³¹, F. Pisani⁴⁸, A. Piucci¹⁷, Resmi P.K¹⁰, V. Placinta³⁷, J. Plews⁵³, M. Plo Casasus⁴⁶, F. Polci¹³, M. Poli Lener²³, M. Poliakov⁶⁸, A. Poluektov¹⁰, N. Polukhina^{81,b}, I. Polyakov⁶⁸, E. Polycarpo², G.J. Pomery⁵⁴, S. Ponce⁴⁸, D. Popov^{5,48}, S. Popov⁴², S. Poslavskii⁴⁴, K. Prasanth³⁴, L. Promberger⁴⁸, C. Prouve⁴⁶, V. Pugatch⁵², H. Pullen⁶³, G. Punzi^{29,m}, W. Qian⁵, J. Qin⁵, R. Quagliani¹³, B. Quintana⁸, N.V. Raab¹⁸, R.I. Rabadan Trejo¹⁰, B. Rachwal³⁵, J.H. Rademacker⁵⁴, M. Rama²⁹, M. Ramos Pernas⁵⁶, M.S. Rangel², F. Ratnikov^{42,82}, G. Raven³³, M. Reboud⁸, F. Redi⁴⁹, F. Reiss¹³, C. Remon Alepuz⁴⁷, Z. Ren³, V. Renaudin⁶³, R. Ribatti²⁹, S. Ricciardi⁵⁷, D.S. Richards⁵⁷, K. Rinnert⁶⁰, P. Robbe¹¹, A. Robert¹³, G. Robertson⁵⁸, A.B. Rodrigues⁴⁹, E. Rodrigues⁶⁰, J.A. Rodriguez Lopez⁷⁴, A. Rollings⁶³, P. Roloff⁴⁸, V. Romanovskiy⁴⁴, M. Romero Lamas⁴⁶, A. Romero Vidal⁴⁶, J.D. Roth⁸⁵, M. Rotondo²³, M.S. Rudolph⁶⁸, T. Ruf⁴⁸, J. Ruiz Vidal⁴⁷, A. Ryzhikov⁸², J. Ryzka³⁵, J.J. Saborido Silva⁴⁶, N. Sagidova³⁸, N. Sahoo⁵⁶, B. Saitta^{27,e}, D. Sanchez Gonzalo⁴⁵, C. Sanchez Gras³², R. Santacesaria³¹, C. Santamarina Rios⁴⁶, M. Santimaria²³, E. Santovetti^{30,j}, D. Saranin⁸¹, G. Sarpis⁵⁹, M. Sarpis⁷⁵, A. Sarti³¹, C. Satriano^{31,p}, A. Satta³⁰, M. Saur⁵, D. Savrina^{39,40}, H. Sazak⁹, L.G. Scantlebury Smead⁶³, S. Schael¹⁴, M. Schellenberg¹⁵, M. Schiller⁵⁹, H. Schindler⁴⁸, M. Schmelling¹⁶, B. Schmidt⁴⁸, O. Schneider⁴⁹, A. Schopper⁴⁸, M. Schubiger³², S. Schulte⁴⁹, M.H. Schune¹¹, R. Schwemmer⁴⁸, B. Sciascia²³, A. Sciubba³¹, S. Sellam⁴⁶, A. Semennikov³⁹, M. Senghi Soares³³, A. Sergi^{53,48}, N. Serra⁵⁰, L. Sestini²⁸, A. Seuthe¹⁵, P. Seyfert⁴⁸, D.M. Shangase⁸⁵, M. Shapkin⁴⁴, I. Shchemerov⁸¹, L. Shchutska⁴⁹, T. Shears⁶⁰, L. Shekhtman^{43,u}, Z. Shen⁴, V. Shevchenko⁸⁰, E.B. Shields^{25,i}, E. Shmanin⁸¹, J.D. Shupperd⁶⁸, B.G. Siddi²¹, R. Silva Coutinho⁵⁰, G. Simi²⁸, S. Simone^{19,c}, I. Skiba^{21,f}, N. Skidmore⁶², T. Skwarnicki⁶⁸, M.W. Slater⁵³, J.C. Smallwood⁶³, J.G. Smeaton⁵⁵, A. Smetkina³⁹, E. Smith¹⁴, M. Smith⁶¹, A. Snoch³², M. Soares²⁰, L. Soares Lavra⁹, M.D. Sokoloff⁶⁵, F.J.P. Soler⁵⁹, A. Solovov³⁸, I. Solovye³⁸, F.L. Souza De Almeida², B. Souza De Paula², B. Spaan¹⁵, E. Spadaro Norella^{26,n}, P. Spradlin⁵⁹, F. Stagni⁴⁸, M. Stahl⁶⁵, S. Stahl⁴⁸, P. Stefko⁴⁹, O. Steinkamp^{50,81}, S. Stemmler¹⁷, O. Stenyakin⁴⁴, H. Stevens¹⁵, S. Stone⁶⁸, M.E. Stramaglia⁴⁹, M. Straticic³⁷, D. Strelakina⁸¹, S. Strokov⁸³, F. Suljik⁶³, J. Sun²⁷, L. Sun⁷³, Y. Sun⁶⁶, P. Svihra⁶², P.N. Swallow⁵³, K. Swientek³⁵, A. Szabelski³⁶, T. Szumlak³⁵, M. Szymanski⁴⁸, S. Taneja⁶², F. Teubert⁴⁸, E. Thomas⁴⁸, K.A. Thomson⁶⁰, M.J. Tilley⁶¹, V. Tisserand⁹, S. T'Jampens⁸, M. Tobin⁶, S. Tolk⁴⁸, L. Tomassetti^{21,f}, D. Torres Machado¹, D.Y. Tou¹³, M. Traill⁵⁹, M.T. Tran⁴⁹, E. Trifonova⁸¹, C. Trippl⁴⁹, G. Tuci^{29,m}, A. Tully⁴⁹, N. Tuning³², A. Ukleja³⁶, D.J. Unverzagt¹⁷, A. Usachov³², A. Ustyuzhanin^{42,82}, U. Uwer¹⁷, A. Vagner⁸³, V. Vagnoni²⁰, A. Valassi⁴⁸, G. Valenti²⁰, N. Valls Canudas⁴⁵, M. van Beuzekom³², E. van Herwijnen⁸¹, C.B. Van Hulse¹⁸, M. van Veghel⁷⁸, R. Vazquez Gomez⁴⁶, P. Vazquez Regueiro⁴⁶, C. Vázquez Sierra⁴⁸, S. Vecchi²¹, J.J. Velthuis⁵⁴, M. Veltri^{22,o}, A. Venkateswaran⁶⁸, M. Veronesi³², M. Vesterinen⁵⁶, D. Vieira⁶⁵, M. Vieites Diaz⁴⁹, H. Viemann⁷⁶, X. Vilasis-Cardona⁸⁴, E. Vilella Figueras⁶⁰, P. Vincent¹³,

G. Vitali²⁹, A. Vollhardt⁵⁰, D. Vom Bruch¹³, A. Vorobyev³⁸, V. Vorobyev^{43,u}, N. Voropaev³⁸, R. Waldi⁷⁶, J. Walsh²⁹, C. Wang¹⁷, J. Wang³, J. Wang⁷³, J. Wang⁴, J. Wang⁶, M. Wang³, R. Wang⁵⁴, Y. Wang⁷, Z. Wang⁵⁰, H.M. Wark⁶⁰, N.K. Watson⁵³, S.G. Weber¹³, D. Websdale⁶¹, C. Weisser⁶⁴, B.D.C. Westhenry⁵⁴, D.J. White⁶², M. Whitehead⁵⁴, D. Wiedner¹⁵, G. Wilkinson⁶³, M. Wilkinson⁶⁸, I. Williams⁵⁵, M. Williams^{64,69}, M.R.J. Williams⁵⁸, F.F. Wilson⁵⁷, W. Wislicki³⁶, M. Witek³⁴, L. Witola¹⁷, G. Wormser¹¹, S.A. Wotton⁵⁵, H. Wu⁶⁸, K. Wyllie⁴⁸, Z. Xiang⁵, D. Xiao⁷, Y. Xie⁷, A. Xu⁴, J. Xu⁵, L. Xu³, M. Xu⁷, Q. Xu⁵, Z. Xu⁵, Z. Xu⁴, D. Yang³, Y. Yang⁵, Z. Yang³, Z. Yang⁶⁶, Y. Yao⁶⁸, L.E. Yeomans⁶⁰, H. Yin⁷, J. Yu⁷¹, X. Yuan⁶⁸, O. Yushchenko⁴⁴, K.A. Zarebski⁵³, M. Zavertyaev^{16,b}, M. Zdybal³⁴, O. Zenaiev⁴⁸, M. Zeng³, D. Zhang⁷, L. Zhang³, S. Zhang⁴, Y. Zhang⁴, Y. Zhang⁶³, A. Zhelezov¹⁷, Y. Zheng⁵, X. Zhou⁵, Y. Zhou⁵, X. Zhu³, V. Zhukov^{14,40}, J.B. Zonneveld⁵⁸, S. Zucchelli^{20,d}, D. Zuliani²⁸, G. Zunica⁶².

¹*Centro Brasileiro de Pesquisas Físicas (CBPF), Rio de Janeiro, Brazil*

²*Universidade Federal do Rio de Janeiro (UFRJ), Rio de Janeiro, Brazil*

³*Center for High Energy Physics, Tsinghua University, Beijing, China*

⁴*School of Physics State Key Laboratory of Nuclear Physics and Technology, Peking University, Beijing, China*

⁵*University of Chinese Academy of Sciences, Beijing, China*

⁶*Institute Of High Energy Physics (IHEP), Beijing, China*

⁷*Institute of Particle Physics, Central China Normal University, Wuhan, Hubei, China*

⁸*Univ. Grenoble Alpes, Univ. Savoie Mont Blanc, CNRS, IN2P3-LAPP, Annecy, France*

⁹*Université Clermont Auvergne, CNRS/IN2P3, LPC, Clermont-Ferrand, France*

¹⁰*Aix Marseille Univ, CNRS/IN2P3, CPPM, Marseille, France*

¹¹*Université Paris-Saclay, CNRS/IN2P3, IJCLab, Orsay, France*

¹²*Laboratoire Leprince-ringuet (lir), Palaiseau, France*

¹³*LPNHE, Sorbonne Université, Paris Diderot Sorbonne Paris Cité, CNRS/IN2P3, Paris, France*

¹⁴*I. Physikalisches Institut, RWTH Aachen University, Aachen, Germany*

¹⁵*Fakultät Physik, Technische Universität Dortmund, Dortmund, Germany*

¹⁶*Max-Planck-Institut für Kernphysik (MPIK), Heidelberg, Germany*

¹⁷*Physikalisches Institut, Ruprecht-Karls-Universität Heidelberg, Heidelberg, Germany*

¹⁸*School of Physics, University College Dublin, Dublin, Ireland*

¹⁹*INFN Sezione di Bari, Bari, Italy*

²⁰*INFN Sezione di Bologna, Bologna, Italy*

²¹*INFN Sezione di Ferrara, Ferrara, Italy*

²²*INFN Sezione di Firenze, Firenze, Italy*

²³*INFN Laboratori Nazionali di Frascati, Frascati, Italy*

²⁴*INFN Sezione di Genova, Genova, Italy*

²⁵*INFN Sezione di Milano-Bicocca, Milano, Italy*

²⁶*INFN Sezione di Milano, Milano, Italy*

²⁷*INFN Sezione di Cagliari, Monserrato, Italy*

²⁸*Università degli Studi di Padova, Università e INFN, Padova, Padova, Italy*

²⁹*INFN Sezione di Pisa, Pisa, Italy*

³⁰*INFN Sezione di Roma Tor Vergata, Roma, Italy*

³¹*INFN Sezione di Roma La Sapienza, Roma, Italy*

³²*Nikhef National Institute for Subatomic Physics, Amsterdam, Netherlands*

³³*Nikhef National Institute for Subatomic Physics and VU University Amsterdam, Amsterdam, Netherlands*

³⁴*Henryk Niewodniczanski Institute of Nuclear Physics Polish Academy of Sciences, Kraków, Poland*

³⁵*AGH - University of Science and Technology, Faculty of Physics and Applied Computer Science, Kraków, Poland*

³⁶*National Center for Nuclear Research (NCBJ), Warsaw, Poland*

³⁷*Horia Hulubei National Institute of Physics and Nuclear Engineering, Bucharest-Magurele, Romania*

³⁸*Petersburg Nuclear Physics Institute NRC Kurchatov Institute (PNPI NRC KI), Gatchina, Russia*

³⁹*Institute of Theoretical and Experimental Physics NRC Kurchatov Institute (ITEP NRC KI), Moscow,*

Russia

- ⁴⁰Institute of Nuclear Physics, Moscow State University (SINP MSU), Moscow, Russia
⁴¹Institute for Nuclear Research of the Russian Academy of Sciences (INR RAS), Moscow, Russia
⁴²Yandex School of Data Analysis, Moscow, Russia
⁴³Budker Institute of Nuclear Physics (SB RAS), Novosibirsk, Russia
⁴⁴Institute for High Energy Physics NRC Kurchatov Institute (IHEP NRC KI), Protvino, Russia, Protvino, Russia
⁴⁵ICCUB, Universitat de Barcelona, Barcelona, Spain
⁴⁶Instituto Galego de Física de Altas Enerxías (IGFAE), Universidade de Santiago de Compostela, Santiago de Compostela, Spain
⁴⁷Instituto de Física Corpuscular, Centro Mixto Universidad de Valencia - CSIC, Valencia, Spain
⁴⁸European Organization for Nuclear Research (CERN), Geneva, Switzerland
⁴⁹Institute of Physics, Ecole Polytechnique Fédérale de Lausanne (EPFL), Lausanne, Switzerland
⁵⁰Physik-Institut, Universität Zürich, Zürich, Switzerland
⁵¹NSC Kharkiv Institute of Physics and Technology (NSC KIPT), Kharkiv, Ukraine
⁵²Institute for Nuclear Research of the National Academy of Sciences (KINR), Kyiv, Ukraine
⁵³University of Birmingham, Birmingham, United Kingdom
⁵⁴H.H. Wills Physics Laboratory, University of Bristol, Bristol, United Kingdom
⁵⁵Cavendish Laboratory, University of Cambridge, Cambridge, United Kingdom
⁵⁶Department of Physics, University of Warwick, Coventry, United Kingdom
⁵⁷STFC Rutherford Appleton Laboratory, Didcot, United Kingdom
⁵⁸School of Physics and Astronomy, University of Edinburgh, Edinburgh, United Kingdom
⁵⁹School of Physics and Astronomy, University of Glasgow, Glasgow, United Kingdom
⁶⁰Oliver Lodge Laboratory, University of Liverpool, Liverpool, United Kingdom
⁶¹Imperial College London, London, United Kingdom
⁶²Department of Physics and Astronomy, University of Manchester, Manchester, United Kingdom
⁶³Department of Physics, University of Oxford, Oxford, United Kingdom
⁶⁴Massachusetts Institute of Technology, Cambridge, MA, United States
⁶⁵University of Cincinnati, Cincinnati, OH, United States
⁶⁶University of Maryland, College Park, MD, United States
⁶⁷Los Alamos National Laboratory (LANL), Los Alamos, United States
⁶⁸Syracuse University, Syracuse, NY, United States
⁶⁹School of Physics and Astronomy, Monash University, Melbourne, Australia, associated to ⁵⁶
⁷⁰Pontifícia Universidade Católica do Rio de Janeiro (PUC-Rio), Rio de Janeiro, Brazil, associated to ²
⁷¹Physics and Micro Electronic College, Hunan University, Changsha City, China, associated to ⁷
⁷²Guangdong Provincial Key Laboratory of Nuclear Science, Institute of Quantum Matter, South China Normal University, Guangzhou, China, associated to ³
⁷³School of Physics and Technology, Wuhan University, Wuhan, China, associated to ³
⁷⁴Departamento de Física, Universidad Nacional de Colombia, Bogota, Colombia, associated to ¹³
⁷⁵Universität Bonn - Helmholtz-Institut für Strahlen und Kernphysik, Bonn, Germany, associated to ¹⁷
⁷⁶Institut für Physik, Universität Rostock, Rostock, Germany, associated to ¹⁷
⁷⁷INFN Sezione di Perugia, Perugia, Italy, associated to ²¹
⁷⁸Van Swinderen Institute, University of Groningen, Groningen, Netherlands, associated to ³²
⁷⁹Universiteit Maastricht, Maastricht, Netherlands, associated to ³²
⁸⁰National Research Centre Kurchatov Institute, Moscow, Russia, associated to ³⁹
⁸¹National University of Science and Technology "MISIS", Moscow, Russia, associated to ³⁹
⁸²National Research University Higher School of Economics, Moscow, Russia, associated to ⁴²
⁸³National Research Tomsk Polytechnic University, Tomsk, Russia, associated to ³⁹
⁸⁴DS4DS, La Salle, Universitat Ramon Llull, Barcelona, Spain, associated to ⁴⁵
⁸⁵University of Michigan, Ann Arbor, United States, associated to ⁶⁸

^aUniversidade Federal do Triângulo Mineiro (UFTM), Uberaba-MG, Brazil

^bP.N. Lebedev Physical Institute, Russian Academy of Science (LPI RAS), Moscow, Russia

^cUniversità di Bari, Bari, Italy

^dUniversità di Bologna, Bologna, Italy

^eUniversità di Cagliari, Cagliari, Italy

^fUniversità di Ferrara, Ferrara, Italy

- ^g *Università di Firenze, Firenze, Italy*
^h *Università di Genova, Genova, Italy*
ⁱ *Università di Milano Bicocca, Milano, Italy*
^j *Università di Roma Tor Vergata, Roma, Italy*
^k *AGH - University of Science and Technology, Faculty of Computer Science, Electronics and Telecommunications, Kraków, Poland*
^l *Università di Padova, Padova, Italy*
^m *Università di Pisa, Pisa, Italy*
ⁿ *Università degli Studi di Milano, Milano, Italy*
^o *Università di Urbino, Urbino, Italy*
^p *Università della Basilicata, Potenza, Italy*
^q *Scuola Normale Superiore, Pisa, Italy*
^r *Università di Modena e Reggio Emilia, Modena, Italy*
^s *Università di Siena, Siena, Italy*
^t *MSU - Iligan Institute of Technology (MSU-IIT), Iligan, Philippines*
^u *Novosibirsk State University, Novosibirsk, Russia*
^v *Department of Physics and Astronomy, Uppsala University, Uppsala, Sweden*